Infrared properties of epitaxial $La_{2-x}Sr_xCuO_4$ thin films in the normal and superconducting states

F. Gao, D. B. Romero,* and D. B. Tanner
Department of Physics, University of Florida, Gainesville, Florida 32611

J. Talvacchio and M. G. Forrester
Westinghouse Science and Technology Center, Pittsburgh, Pennsylvania 15235

(Received 23 July 1992; revised manuscript received 14 September 1992)

The CuO_2-plane optical reflectance of superconducting $La_{2-x}Sr_xCuO_4$ thin films ($T_c \simeq 31$ K) has been measured over a wide frequency and temperature range. The optical conductivity in the normal state is well described by a temperature-dependent weak-coupling ($\lambda \approx 0.25$) free-carrier term plus an overdamped, weakly temperature-dependent, midinfrared component. The free-carrier plasma frequency is nearly constant, $\omega_{pD} = 6300$ cm^{-1}, whereas the relaxation rate varies linearly with temperature above T_c. In the superconducting state, according to our two-component approach, most of the Drude oscillator strength condenses to a $\delta(\omega)$ function. A two-fluid analysis gives a rapid drop in the quasiparticle damping rate below T_c. A reasonable estimate (~ 2750 Å) for the *ab*-plane London penetration depth is obtained from the superfluid density. We observe that the midinfrared strength increases below T_c, suggesting that some ($\sim 15\%$) of the free carriers do not condense into superconducting pairs and may have a strong interaction with pair-breaking excitations. Two absorption edges around 80 cm^{-1} ($3.7\ k_B T_c$) and 400 cm^{-1} ($18\ k_B T_c$) are seen but neither is assigned to the superconducting gap. Comparisons with a one-component picture described by a frequency-dependent scattering rate and effective mass are made and discussed. The far-infrared *ab*-plane phonons show systematic changes with temperature, which are associated with the structural transition near 250 K.

I. INTRODUCTION

Since the discovery of high-temperature superconductors (HTSC),[1,2] tremendous efforts have occurred in the studies of these cuprate oxides. Most optical studies have concentrated on the 90-K transition temperature $YBa_2Cu_3O_{7-\delta}$ (YBCO) system, which contains both CuO_2 planes and CuO chains. (For reviews, see Refs. 3–6). It has been observed, however, that the quasi-one-dimensional CuO chains in YBCO have a substantial contribution to the optical conductivity,[7,8] which has complicated the analysis of this material. In contrast, the $La_{2-x}Sr_xCuO_4$ (LSCO) system, which contains only single CuO_2 layers, has been studied in most cases in sintered polycrystalline samples.[9–15] Because the LSCO materials are strongly anisotropic, it is difficult to determine the intrinsic nature of the CuO_2 layers from measurements of polycrystalline samples. A few optical measurements, mostly restricted to room temperature, on LSCO single crystals or thin films have been made,[16–21] but we are not aware of a systematic temperature-dependent optical study on the oriented samples of this material.

It is widely believed that the electron-phonon interaction plays a minor role in the superconductivity for YBCO materials. However, a significant isotope shift ($\alpha \simeq 0.2$) due to partial substitute of ^{18}O for ^{16}O in $La_{1.85}Sr_{0.15}CuO_4$ has been observed and interpreted as evidence for strong electron-phonon coupling.[22,23] This implies that phonons may still play an important role, if not a key role, in the pairing mechanism. On the other hand, the observed linear behavior of the dc resistivity for LSCO up to 1100 K implies a weak electron-phonon coupling for the free carriers.[24]

A lot of effort has been made in recent years to study the non-Drude response in the midinfrared (MIR) region and to discover the superconducting energy gap. It has been observed that the MIR absorption is absent in the undoped parent compounds such as La_2CuO_4 and $YBa_2Cu_3O_6$. For $La_{2-x}Sr_xCuO_4$, Uchida *et al.*[21] have reported that the MIR absorption band develops with increasing dopant concentration and then exhibits a saturation in the higher compositional range $0.1 \le x \le 0.25$. Similar effects are observed in doping of *n*-type $Pr_{2-x}Ce_xCuO_4$ by Cooper *et al.*[25] As a consequence of the redistribution of the O $2p$ and Cu $3d$ orbitals upon doping, spectral weight is rapidly transferred from the in-plane O $2p \rightarrow$ Cu $3d$ charge-transfer (CT) excitations above 2 eV to the free-carrier absorption (Drude band) and the low-energy excitations (MIR band) below 1.5 eV. Therefore, both the Drude and MIR absorptions in HTSC appear to be related to the introduction of holes on the CuO_2 layers (or CuO chains) by doping. For LSCO, the CT gap becomes weaker or fills in and the phonons are obscured as holes are added upon substituting Sr^{2+} for La^{3+}. In contrast to these changes, the plasma minimum in the reflectance is pinned at 0.9 eV and insensitive to the dopant concentration.[14,15,26,27]

Although there is fairly good agreement among various groups for the optical conductivity of the high-T_c copper oxides, the interpretation of these results still remains controversial. In no case can the normal-state infrared

conductivity be described by a simple Drude model. In many studies,[3–5,28–33] this non-Drude conductivity has been described by a two-component approach: a narrow, strongly temperature-dependent Drude absorption centered at the origin and a broad, nearly temperature-independent midinfrared band. The Drude absorption is due to the free carriers which are responsible for the dc transport and which condense into a superfluid below T_c whereas the MIR absorption is due to the bound carriers which have a semiconductorlike gap. An alternative is a single-component approach: all of the infrared absorption is due to one type of carrier, with a strong frequency dependence in the scattering rate and effective mass. This approach also leads to a broad range of optically inactive excitations in the midinfrared region, and has been described in the framework of the "marginal Fermi liquid"[34] (MFL) and "nested Fermi liquid" (NFL).[35]

In this paper, we present the in-plane spectra of reflectance $\mathcal{R}(\omega,T)$ and conductivity $\sigma(\omega,T)$ of a high-quality $La_{2-x}Sr_xCuO_4$ film over a wide frequency range of 30–40 000 cm^{-1} (4 meV–5 eV) and for temperatures between 5 and 350 K. We make an extensive optical study on the infrared dynamics of the film. In Sec. II, the sample preparation and the characteristic transport properties are discussed. We also describe in detail the optical measurement technique and discuss the uncertainties in the Kramers-Kronig (KK) analysis. Section III presents the spectra of reflectance and other optical functions derived from the KK analysis. Details of the infrared phonons and optical conductivity $\sigma(\omega)$ in the normal and superconducting states are discussed. Comparisons of the normal-state data to both two- and one-compound descriptions of the optical dielectric function are also made in Sec. III. Finally, the conclusions are summarized in Sec. IV.

II. EXPERIMENT

A. Sample characteristics

$La_{2-x}Sr_xCuO_4$ films were prepared by off-axis dc magnetron sputtering. Details of sample preparation and dc transport properties have been described previously.[36] Films were grown on $SrTiO_3$ or $LaAlO_3$ substrates. Both kinds of substrates have a perovskite structure which enables a good lattice match with the films. Parameters of the samples are summarized in Table I. Thinner films (270 nm thickness) were transparent enough that some features of the substrate could be seen in the reflectance spectra. Consequently, the work described here will focus on an especially thick film with thickness greater than the electromagnetic penetration depth ($d > \delta$) to avoid the substrate complications. This film, grown on the (100) face of a $SrTiO_3$ substrate, has dimensions of 10 mm×10 mm×820 nm. Figure 1 shows an x-ray-diffraction pattern for a film grown at the same time as the film used for infrared measurements, showing that it is highly *ab*-plane oriented. In addition to its *c*-axis texture, the film is epitaxial. That is, the [100] and [010] directions, which lie in the plane of the film, are parallel to the [100] and [010] directions in the substrate. The *ab*-plane dc resistivity, shown in Fig. 2, displays a sharp

TABLE I. $La_{2-x}Sr_xCuO_4$ thin-film characteristics.

Sample no.	Thickness (nm)	Area (mm^2)	x	T_c (K)	ΔT_c (K)	Substrate
1,2	270	6.3×6.3	0.15	27	1.5	$LaAlO_3$
3	820	10×10	0.17	31	1.5	$SrTiO_3$

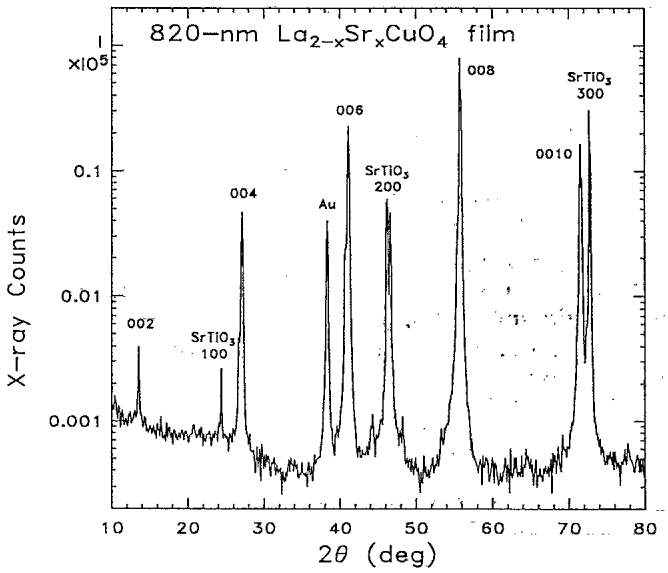

FIG. 1. X-ray-diffraction pattern for a $La_{2-x}Sr_xCuO_4$ thin film grown at the same time as the one used this work. The film was grown on a $SrTiO_3$ substrate, and the growth orientation can be seen in this figure.

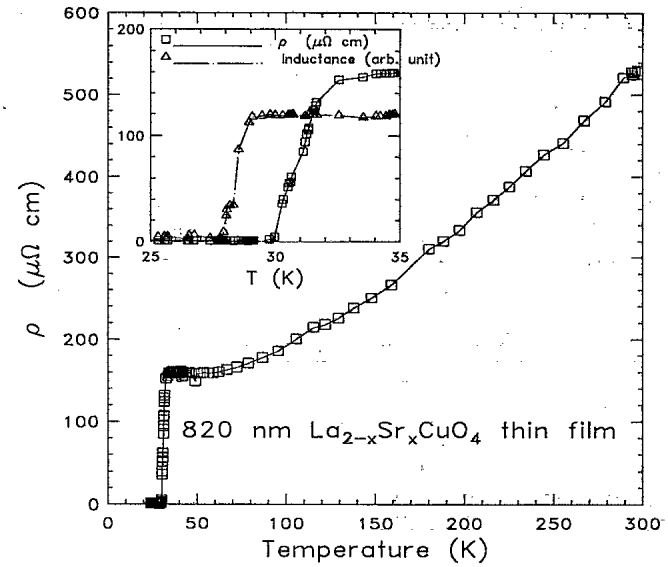

FIG. 2. Resistivity in the *ab* plane, as a function of temperature, for the same $La_{2-x}Sr_xCuO_4$ film ($x \sim 0.17$) as shown in Fig. 1. The inset shows an expanded view of the region near T_c for the same sample and compares the resistive transition to the inductive transition. The lines connecting points are guides to the eye.

superconducting transition near $T_c = 31$ K with a transition width $\Delta T_c \simeq 1.5$ K. The normal-state resistivity is roughly linear in temperature with a nearly zero intercept, i.e., of the form of $\rho(T) = \rho_0 + \alpha T$ ($\alpha \sim 1.2$ $\mu\Omega$ cm/K). Deviations from this behavior are evident in the plateau below ~ 100 K. The inset in Fig. 2 shows that the inductive transition, as measured by the change of inductance of a coil placed against the film, is at approximately 2-K lower temperature than the resistive transition and has about the same transition width. The composition of the film is at an optimum value ($x \sim 0.17$) for the superconductivity. The resistivity is consistent with the published reports of good quality LSCO crystals.[20,21]

B. Infrared measurements and uncertainties

The reflectance measurements were performed using two spectrometers with a variety of light sources, beamsplitters, and detectors for different overlapping frequency ranges. The angle of incidence of the incident light was about 11° from the surface normal, so that the electric field of the infrared radiation was dominantly parallel to the *ab* plane. Reflectance spectra in the far- and midinfrared range 30–4000 cm^{-1} (4–500 meV) were measured using a Bruker 113 v fast scanning Fourier transform interferometer with a 4.2-K bolometer detector (30–600 cm^{-1}) and a B-doped Si photoconductor (450–4000 cm^{-1}). At higher frequencies of 1000–40 000 cm^{-1} (0.125–5 eV), the reflectance was measured with a Perkin Elmer 16U grating monochromator. The reflectance was calibrated with a reference mirror of 2000-Å-thick aluminum evaporated on an optically polished glass substrate. The sample and Al mirror reference were mounted on a helium-cooled cold tip, along with a silicon thermometer and a resistance heater, to allow the temperature to be varied from 5 to 350 K. The sample and reference could be exchanged by rotating the cryostat.

As the overall scale of the reflectance is very crucial to the analysis of HTSC, we carefully tested the stability and measured the absolute reflectance at each temperature. Thermal contraction of the sample holder and position variation between the sample and reference were also compensated for. In order to study the temperature dependence of the midinfrared band and the plasma edge, we measured the reflectance at each temperature up to 4000 cm^{-1} (0.5 eV), and at selected temperatures up to 40 000 cm^{-1} (5 eV). The coincidence of spectra in each of the overlap frequency range was usually within 0.5%. As the film thickness (820 nm) was much greater than the penetration-skin depth (~ 250 nm), features attributable to the $SrTiO_3$ substrate effect were not detected. Because the sample surface was extremely smooth and shiny, specular reflection was assumed and there was no need to coat the sample with a metal film to correct for diffuse scattering losses. Also, the large sample area (1×1 cm^2) enabled us to obtain a high signal-to-noise ratio, making it unnecessary to smooth the data for analysis.

The experimental uncertainty in our reflectance measurements is estimated to be $\pm 0.5\%$. This error arises mainly from the difficulty in establishing precise optical alignment as the reference and the sample are interchanged, and partly from the slight temperature dependence of the Al reflectance at low frequencies. This small uncertainty in $\mathcal{R}(\omega)$, however, will cause a larger propagated error at low frequencies in the optical conductivity $\sigma(\omega)$ generated by the Kramers-Kronig transformation.

C. Kramers-Kronig analysis

After obtaining satisfactory results for a wide range of reflectance spectra $\mathcal{R}(\omega)$, we have confidence in using the Kramers-Kronig transform to determine the real part of the optical conductivity $\sigma_1(\omega)$, a more fundamental quantity than $\mathcal{R}(\omega)$ for describing particle-hole excitations of a material by the absorption of photons of energy $\hbar\omega$. In principle, the KK integral requires a knowledge of $\mathcal{R}(\omega)$ at all frequencies.[37] Thus, reasonable and careful extrapolations of the reflectance beyond the measured range must be made.

1. High-frequency extrapolation

The high-frequency extrapolation usually has significant influence on the results, primarily on the sum rule derived from the optical conductivity. This effect has been reduced by merging our data to the reflectance spectra of Tajima *et al.*,[19] which extend up to 37 eV (300 000 cm^{-1}). We find their spectra are in excellent agreement (within $\pm 0.8\%$ in absolute reflectance) with our high-frequency data at room temperature.

After careful measurements, however, we observe a significant decrease in the overall level of $\mathcal{R}(\omega)$ at frequencies above the plasma edge (~ 7000 cm^{-1}) as the temperature is lowered below 250 K. This decrease persists up to 40 000 cm^{-1}, the upper limit of our experimental data, the reflectance at 250 K being about 80% of that at room temperature in this frequency region. However, as the temperature is further decreased below 250 K, aside from the steepening of the plasma edge, there is very little temperature dependence down to 5 K in this high-frequency region as shown in Fig. 3. We have carefully repeated the measurements several times and found this behavior reproducible in both the cooling and warming process. At the same time, we have observed no change at all temperatures in the signal level reflected from the Al reference which has been mounted near the sample. In addition, the reflectance remains unchanged as the sample is heated up from 300 to 350 K. These tests have convinced us that the extraneous influence such as thermal expansion-contraction of the sample holder or condensation of water on the sample can be ruled out. We therefore have readjusted the high-frequency room-temperature reflectivity given by Tajima *et al.*[19] with a factor of 5% increase in the range 5–8 eV, but no change above this range, before appending it to our data for temperatures below 250 K. After doing so, we have assumed $\mathcal{R}(\omega) \sim \omega^{-4}$, a free-electron asymptotic behavior, above 37 eV. These changes preserve the sum rule at 20 eV.

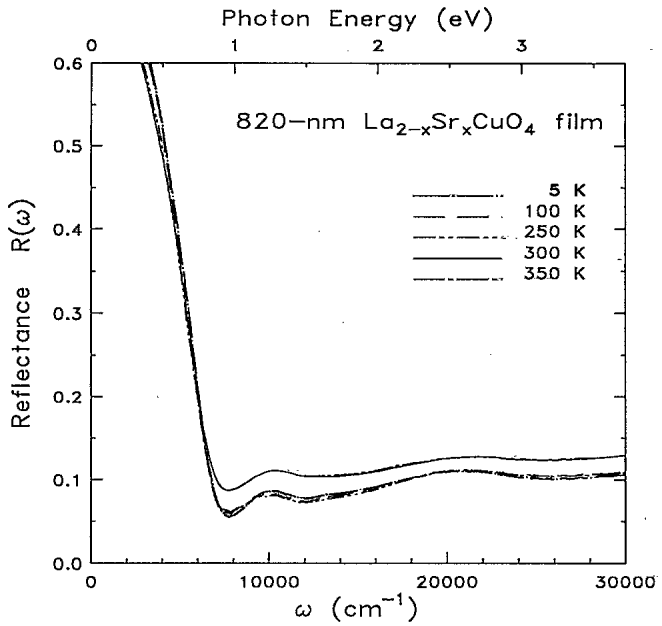

FIG. 3. Temperature dependence of the reflectance in the interband region. There is a remarkable change in $\mathcal{R}(\omega)$ between 300 and 250 K but no appreciable change above or below this temperature range.

2. *Low-frequency extrapolation*

The low-frequency extrapolation is equally important. We find that using the Hagen-Rubens relation, $\mathcal{R}(\omega)=1-A\sqrt{\omega}$, for the normal state leads to a slightly depressed conductivity near the low-frequency end followed by a sharp rise towards zero frequency. This distortion may affect the estimate of the dc conductivity and also of the sum rule, from which we want to find the superconducting condensate by calculating the missing area below T_c. Since the Hagen-Rubens relation, a good approximation for ordinary metals, seems not appropriate for the HTSC because of the presence of phonons and of low-frequency (midinfrared) absorption processes, we make a least-squares fit to the optical conductivity, $\sigma_1(\omega)$, derived from the initial KK transform of $\mathcal{R}(\omega)$ using a two-component dielectric function (Drude plus midinfrared and phonon oscillations):

$$\epsilon(\omega)=-\frac{\omega_{pD}^2}{\omega^2+i\omega/\tau}+\sum_{j=1}^{N}\frac{\omega_{pj}^2}{\omega_j^2-\omega^2-i\omega\gamma_j}+\epsilon_\infty, \quad (1)$$

where the first term is a Drude oscillator described by a plasma frequency ω_{pD} and a relaxation time τ of the free carriers; the second term is a sum of oscillators for midinfrared and phonon absorptions with ω_j, ω_{pj}, and γ_j being the resonant frequency, strength, and width of the jth Lorentz oscillator; and the last term ϵ_∞ is the high-frequency limit of $\epsilon(\omega)$. This last parameter is found from a fit to $\mathcal{R}(\omega)$.

Using the fit parameters, we recalculate the low-frequency reflectance for the normal state. Then, after extending the experimental $\mathcal{R}(\omega)$ with this calculated reflectance, a second KK transform is made. The results of this "second" $\sigma_1(\omega)$ give a more reasonable low-frequency behavior. In the superconducting state, we have used the formula $\mathcal{R}=1-B\omega^4$, as the way that $\mathcal{R}$ goes to unity. For temperatures well below T_c, the low-frequency reflectance is nearly constant, with some noise fluctuations around unity. We have set $\mathcal{R}\equiv 1$ in this region for the KK transformation. As mentioned earlier, the experimental uncertainty in $\mathcal{R}(\omega)$ is about $\Delta\mathcal{R}=\pm 0.5\%$. As $\mathcal{R}(\omega)\rightarrow 1$ at low ω and low T, the KK transform will give propagated error in $\sigma_1(\omega)$—primarily coming from the propagated error in the real index of refraction $n(\omega)$—roughly equal to $\Delta\sigma_1/\sigma_1=[1/(1-\mathcal{R})](\Delta\mathcal{R}/\mathcal{R})$, i.e., the percentage uncertainty in σ_1 is about $1/(1-\mathcal{R})$ times higher than that in $\mathcal{R}$. We will address this issue later.

III. RESULTS AND DISCUSSION

A. Infrared phonons

Figure 3 shows the measured *ab*-plane reflectance $\mathcal{R}(\omega,T)$ of a $La_{2-x}Sr_xCuO_4$ thin film on a linear scale. The low-frequency behavior is shown in Fig. 4 at several temperatures. The inset, which is plotted on a logarithmic frequency scale for the entire measured frequency range at three typical temperatures, illustrates the strongly damped plasma edge around 0.8 eV (6000 cm^{-1}) and the interband features around the visible region. As we can see from Fig. 4, $\mathcal{R}(\omega,T)$ increases over a broad frequency range with decreasing temperature, as expected. A few infrared-active phonons in the *ab*-plane are visible. These phonons are more obvious in the spectrum than in the case of YBCO.[3-5,31-33] This indicates that the LSCO crystal has a lower free-carrier concentration and

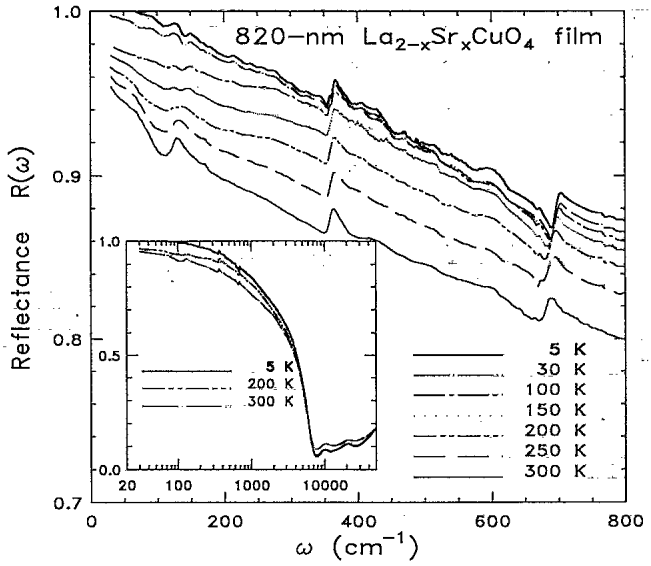

FIG. 4. Measured reflectance $\mathcal{R}(\omega)$ at selected temperatures between 5 and 300 K. The inset shows the same data over the entire measured frequency range (note the logarithmic frequency scale).

a higher vibrational oscillator strength. The phonon parameters can also be extracted from $\sigma_1(\omega)$, the real part of the optical conductivity, shown in Fig. 5. Of the seven IR-active phonon modes ($3A_{2u}+4E_u$) expected at the Γ point for the body-centered tetragonal D_{4h}^{17}-$I4/mmm$ symmetry, three distinct ab-plane E_u modes are observed at 126, 359, and 681 cm^{-1} for $T=300$ K. These eigenenergies are close to those previously reported by Collins *et al.*,[18] 132, 358, and 667 cm^{-1}, from a room-temperature reflectance study of a LSCO single crystal. These three phonons have been assigned as external, bending, and stretching modes, respectively.[38,39] More details regarding the phonon mode assignment have been reported in Ref. 40.

1. Structural phase transition

We note that the lowest phonon mode at $\omega=126$ cm^{-1}, corresponding to an in-plane translational vibration of the La atoms against the CuO_6 octahedron unit, broadens and splits into two distinct modes as T decreases below 250 K. The splitting begins at the tetragonal-to-orthorhombic structural transition which involves a staggered rotation of CuO_6 octahedron. At 200 K, the degeneracy of the two modes is lifted but their energies are so close that they can barely be resolved. The splitting develops upon further cooling as depicted in Fig. 6. Similar results in neutron-scattering measurements have been reported and associated with a soft phonon mode.[41] For comparison, the inset in Fig. 6 shows the results of Keane *et al.*[42] for the in-plane lattice constants of a $La_{1.85}Sr_{0.15}CuO_4$ sample as a function of temperature. The structural distortion is evident in their data at $T \lesssim 200$ K.

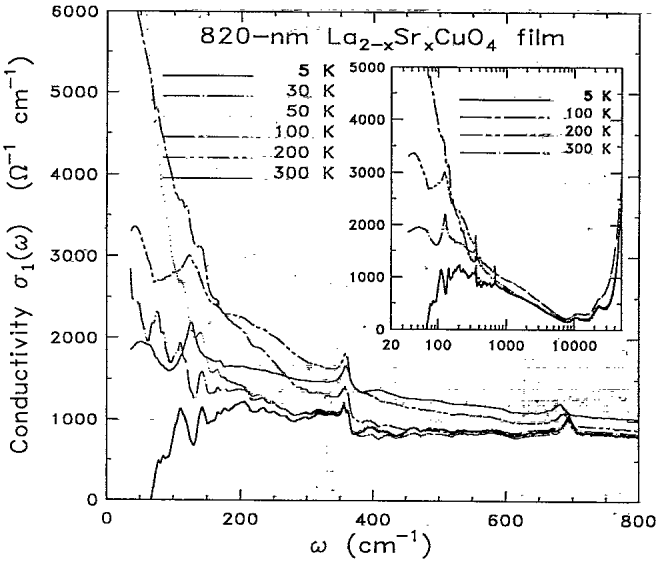

FIG. 5. The real part of the ab-plane conductivity $\sigma_1(\omega)$ derived from the Kramers-Kronig transformation of the reflectance data in Fig. 4. The inset shows the entire measured frequency range.

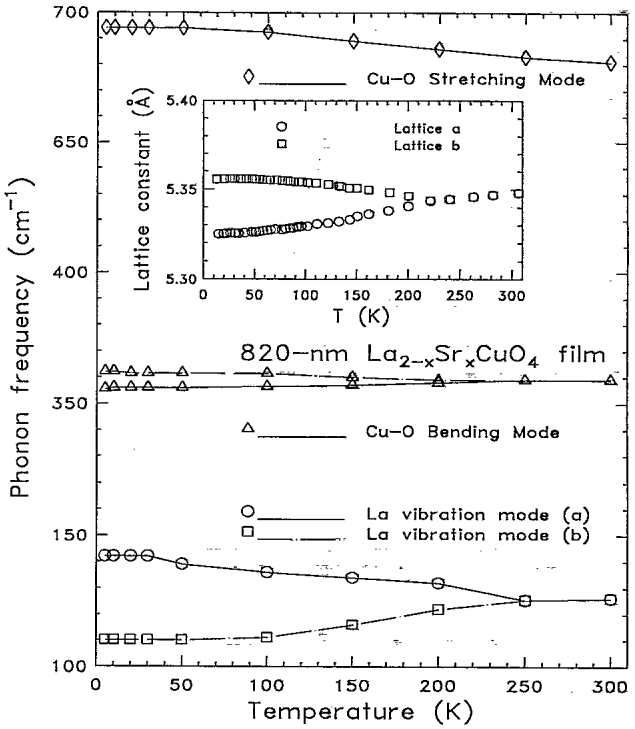

FIG. 6. The in-plane phonon frequency as a function of temperature (the lines are guides to the eye). For comparison, the inset shows the results of Keane *et al.* for the T-dependent ab-plane lattice constants of $La_{1.85}Sr_{0.15}CuO_4$ (Ref. 42).

2. Frequency shift and lifetime

We also observe that the Cu-O stretching mode at 681 cm^{-1} hardens by 13 cm^{-1} as the sample cools from 300 to 100 K, as expected for thermal contraction. It stops shifting, however, upon further cooling. In contrast, the frequency of the Cu-O bending mode at 359 cm^{-1} remains constant at all temperatures yet exhibits a discernible splitting at low T. We thus conclude that the stretching mode is much more sensitive to the Cu-O bond length than the bending mode. Tajima *et al.*[38] have recently found a similar result when they measured the room-temperature phonon frequencies of different cuprates with different lattice constants a but almost the same reduced mass by substituting the La atom by other rare-earth elements. A similar effect has also been observed in the T'-RE_2CuO_4 system by Herr *et al.*[43] In our case the absence of further hardening at lower temperatures is probably due to the fact that the real part of the phonon self-energy $\Sigma_{ph}=\Delta+i\Gamma$ has three contributions:

$$\Delta(T)=\Delta^{(0)}(T)+\Delta^{(1)}(T)+\Delta^{(2)}(T)\ , \qquad (2)$$

where $\Delta^{(0)}$ accounts for thermal expansion, $\Delta^{(1)}$ and $\Delta^{(2)}$ for the cubic and quartic anharmonic terms in the lattice potential, respectively. These contributions are generally of the same order of magnitude but may have different signs. Thus, $\Delta^{(0)}$ may be compensated by the sum of $\Delta^{(1)}+\Delta^{(2)}$ at low temperatures. Another possibility is the saturation of the T dependence of all three contributions

below 100 K. Such an effect has been found in silver and thallium halides.[44] Indeed, Tranquada, Heald, and Moodeneabaugh[45] and Keane *et al.*[42] have observed that the interatomic distances of $La_{2-x}Sr_xCuO_4$ saturate below 100 K.

It has been reported[46,47] that the two lower-lying IR-active phonons at 149 and 190 cm^{-1} for $YBa_2Cu_3O_7$ ceramic samples narrow dramatically but have no softening upon entering into superconducting state. In contrast, the phonons above 275 cm^{-1} exhibit the opposite behavior (i.e., little change in width but apparent softening below T_c). The anomalous, dramatic narrowing in phonon widths for $YBa_2Cu_3O_{7-\delta}$ has been attributed to the disappearance of interaction between electrons and phonons with energies less than the superconducting gap when the electrons condense into Cooper pairs below T_c.[3] The phonon lifetime will increase as a result of decreased probability of colliding with quasiparticles, because the number of quasiparticle excitations decreases rapidly below T_c. The frequency shift has been explained within the framework of conventional strong-coupling theory.[48] It is interesting that such a narrowing effect observed in YBCO ceramic samples has not been seen in single crystals.[49,50] Note in both cases the observed phonons are the *c*-axis modes, because the *ab*-plane phonon modes are screened by the strong plasmon background. The difference between these two cases may be attributed to the fact that $YBa_2Cu_3O_7$ is insulating along the *c* direction hence the *c*-axis modes in the oriented samples do not sense the change when the free carriers condense into the superfluid, whereas the same *c*-axis phonons in the randomly oriented samples may be affected by the *ab*-plane carriers due to intergrain hopping. In any event, we do not see a dramatic T dependence in the observed *ab*-plane phonons for $La_{2-x}Sr_xCuO_4$, perhaps because the lowest phonon mode at 126 cm^{-1} is far above the BCS gap energy, which would be ~ 80 cm^{-1} for a $T_c = 31$-K sample.

B. Two-component approach

Returning to the conductivity spectra shown in Fig. 5, we note that the normal state $\sigma_1(\omega, T)$ at the low-frequency limit is nearly equal to the dc conductivity and exhibits a Drude response. A definite loss of spectral weight can be seen at 30 K for $\omega < 150$ cm^{-1}, implying a shift of weight to the origin accompanying the superconducting condensation. At $T \ll T_c$, the inductive current, governed by the imaginary part of the complex conductivity σ_2, is dominant for $\omega < 150$ cm^{-1}. It diverges as $\omega \to 0$, showing an A/ω dependence as demonstrated in Fig. 7. The constant A is associated with the strength of the superconducting condensate and the London penetration depth. However, when $\omega > 150$ cm^{-1}, σ_2 falls off slowly, deviating significantly from a $1/\omega$ dependence. Above T_c, σ_2 changes slope at low frequencies and extrapolates to the origin; the maximum moves to higher frequency and decreases with increasing temperature, as expected.

In contrast to the simple free-carrier response, at $\omega > 300$ cm^{-1}, the normal-state $\sigma_1(\omega)$ in Fig. 5 decays much more slowly than the ω^{-2} dependence that one expects in a Drude model. Additionally, $\sigma_1(\omega)$ has much weaker temperature dependence at high frequencies than at low frequencies. This "non-Drude" behavior, which is universal for all copper oxide superconductors,[3-6,28-33,51-53] can be described in a two-component picture, in which a narrow (with a width of order k_BT) and strongly T-dependent free carrier (Drude) absorption peaked at $\omega = 0$ combines with a broad bound-carrier (MIR) absorption centered at higher frequencies. According to this picture, the cuprates are viewed as consisting of two types of carriers: free carriers which track the dc conductivity above T_c and which condense to superconducting pairs below T_c, and bound carriers which are responsible for the broad MIR excitation. The dielectric function is made up of four parts:

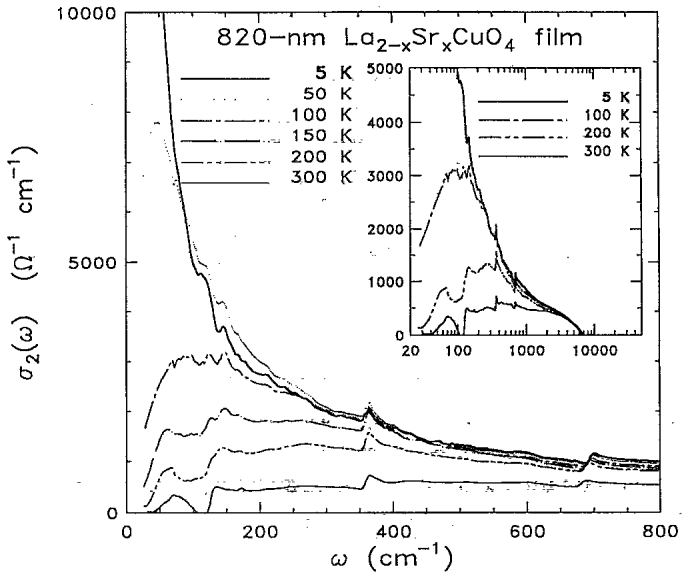

FIG. 7. The imaginary part of the conductivity, $\sigma_2(\omega)$, showing the inductive response. The inset plots the same data in the entire measured frequency range.

$$\epsilon(\omega) = \epsilon_D + \epsilon_{\mathrm{MIR}} + \epsilon_{\mathrm{phonon}} + \epsilon_\infty \ , \tag{3}$$

where ϵ_D is the free carrier or normal Drude interband contribution; ϵ_{MIR} is the bound-carrier contribution; $\epsilon_{\mathrm{phonon}}$ is the phonon contributions, a sum of harmonic oscillators; and ϵ_∞ is the high-frequency contribution.

To decompose the total conductivity into two components, we can assume that the conductivity at 5 K, $\sigma_1(\omega, 5\ \mathrm{K})$, is a good first approximation of $\sigma_{1\mathrm{MIR}}$, namely, $\sigma^{(1)}_{1\mathrm{MIR}} = \sigma_1(\omega, 5\ \mathrm{K})$, for the Drude part is presumed to have collapsed to a $\delta(\omega)$ function. Thus, the Drude conductivity at higher temperatures can be initially estimated by subtracting $\sigma_1(\omega, 5\ \mathrm{K})$ from the experimental $\sigma_1(\omega, T)$, namely, $\sigma^{(1)}_{1D} = \sigma_1 - \sigma^{(1)}_{1\mathrm{MIR}}$. Here the superscripts denote the number of iterations. Since

$$\sigma_{1D} = \frac{1}{4\pi} \frac{\omega_{pD}^2 \tau}{1 + \omega^2 \tau^2} \ , \tag{4}$$

we can determine ω_{pD} and $1/\tau$ from a linear fit to $1/\sigma^{(1)}_{1D}$

vs ω^2. Once ω_{pD} and $1/\tau$ are determined from the slope and the intercept of this straight line, we can again estimate the midinfrared conductivity from the difference between a calculated Drude conductivity and the measured conductivity, namely, $\sigma^{(2)}_{1\mathrm{MIR}} = \sigma_1 - \sigma_{1D}$, where σ_{1D} is *calculated* according to Eq. (4). By averaging $\sigma^{(2)}_{1\mathrm{MIR}}$ at temperatures above T_c, we find the average $\langle \sigma^{(2)}_{1\mathrm{MIR}} \rangle \approx \sigma^{(1)}_{1\mathrm{MIR}}$ [or $\sigma_1(\omega, 5\ \mathrm{K})$], but there are noticeable differences. Therefore, we repeat the above procedure with $\sigma^{(2)}_{1\mathrm{MIR}}$ replacing $\sigma^{(1)}_{1\mathrm{MIR}}$, and find convergence after a few iterations.

1. The free-carrier component: ω_{pD} and τ

Figure 8 illustrates the comparison between the free-carrier contribution, $\sigma_1 - \langle \sigma_{1\mathrm{MIR}} \rangle$, and the calculated Drude conductivity. This figure shows that the conductivity is in good agreement with the ordinary Drude behavior after the MIR component is subtracted. The Drude plasma frequency, $\omega_{pD} = 6300 \pm 100\ \mathrm{cm}^{-1}$, obtained from the above analysis, is essentially T independent, whereas $1/\tau$ is linear in T. Writing $\hbar/\tau = 2\pi\lambda k_B T$, we obtain a weak-coupling value for the coupling constant, $\lambda = 0.25$. This small value of λ is consistent with the observed absence of saturation up to 1100 K for the dc resistivity.[24] Taking the Fermi velocity in the basal plane to be $v_F = 2.2 \times 10^7$ cm/s, as calculated by Allen, Pickett, and Krakauer[54] for $La_{1.85}Sr_{0.15}CuO_4$, and using our relaxation rate we can estimate the mean free path to be

$$l = v_F \tau \approx (110\ \text{Å}) \frac{100\ \mathrm{K}}{T}. \quad (5)$$

At $T = 1000$ K, $l \sim 11$ Å, which is still longer than the interatomic spacing a (here taken to be 3.8 Å, the in-plane lattice constant). The resistivity is expected to saturate if $l \lesssim a$, because the mean free path can no longer be properly defined in this region.[55] On the other hand, at a temperature close to T_c, the mean free path l [e.g., $l_{50\ \mathrm{K}} \sim 220$ Å according to Eq. (5)] is much longer than the coherence length ξ (~ 10 Å). It is this case that places the HTSC in the "clean limit," which, in turn, gives a significant impact on the observability of the superconducting gap.

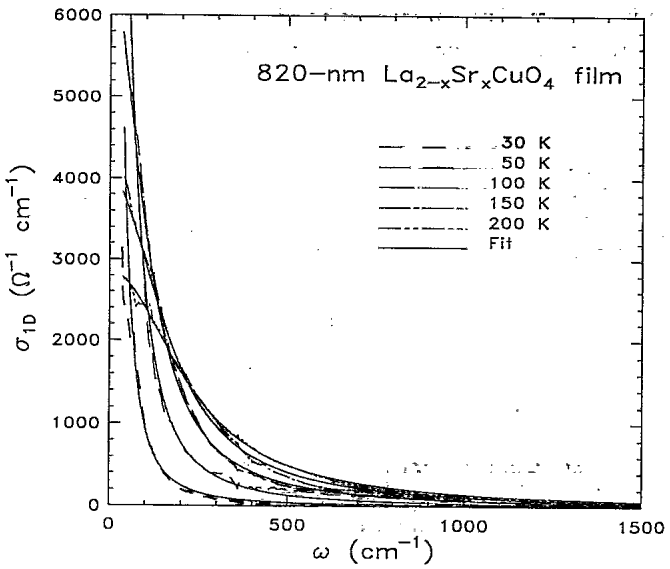

FIG. 8. The Drude conductivity, obtained by subtracting the averaged midinfrared contribution from the total conductivity. The solid curves are Drude fits to the data.

Figure 9 depicts the temperature dependence of $1/\tau$ in comparison with $(1/\tau)_{\mathrm{dc}}$ calculated from the measured four-probe dc resistivity ρ_{dc} and the value of ω_{pD} found above,

$$(1/\tau)_{\mathrm{dc}} = \frac{\omega^2_{pD}}{4\pi} \rho_{\mathrm{dc}}. \quad (6)$$

As seen in Fig. 9, $(1/\tau)_{\mathrm{dc}}$ or ρ_{dc} decreases quasilinearly from room temperature followed by a plateau and then a sudden drop as the temperature approaches T_c whereas the far-infrared scattering rate shows a quasilinear T variation followed by a faster-than-linear drop ($1/\tau \sim T^2$) below T_c. This is evident when the same data are plotted on a log-log scale, as shown in the inset of Fig. 9. The excellent agreement in both the slopes and overall levels between the dc transport and infrared measurements strengthens our confidence in the determination of the normal-state plasma frequency ω_{pD} and scattering rate $1/\tau$. The sudden drop in $1/\tau$ just below T_c is interesting and has received considerable attention recently. Such observations on quasiparticle damping have been reported previously for laser-ablated $YBa_2Cu_3O_{7-\delta}$ films[56,33] and a free-standing $Bi_2Sr_2CaCu_2O_8$ crystal.[57,58] Similar

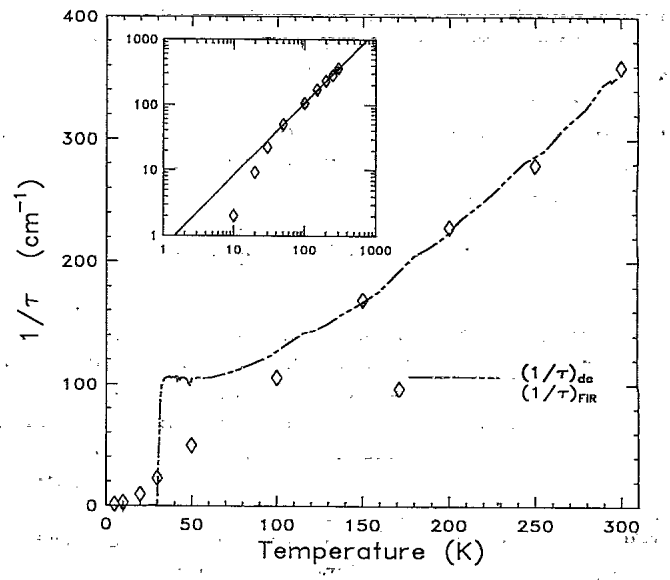

FIG. 9. Drude scattering rate, $1/\tau$, as a function of temperature. For comparison are shown the values obtained from fits to the infrared conductivity (diamond symbols) and the ones estimated from the measured dc resistivity (dashed lines). Note both of these two cases exhibit a small negative intercept due to a slight deviation from T linear dependence. This is illustrated in the inset plotted on a log-log scale. The slope of the solid straight line gives a power of 1.1 instead of 1 to temperature T. Below T_c, the quasiparticle damping rate has a sudden drop and goes roughly as $1/\tau \sim T^2$.

behavior has also been found for YBCO and BSCCO in femtosecond optical transient absorption experiments.[59] This result may suggest that the excitation that scatters the free carriers is also strongly suppressed below T_c, or forms its own gap, as the free carriers condense. Another interpretation is that the number of unoccupied states available near the Fermi levels decreases rapidly as a result of the depression of the density of quasiparticle states near E_F as the gap opens, causing a dramatic decrease in the probability of quasiparticle elastic scattering. Nicol and Carbotte[60] have recently calculated the quasiparticle scattering rate and found such a fast drop within the phenomenological marginal Fermi-liquid model. However, due to the large error bars at low frequencies (below 100 cm^{-1}) and the limited number of temperatures below T_c (31 K) in our data, we are unable to observe a "coherence" peak in $\sigma_1(T)$, as has been calculated by Nicol and Carbotte[60] and found in YBCO by Nuss *et al.*,[61] and in BSCCO by Romero *et al.*[58]

2. *The midinfrared absorption*

Figure 10 presents the MIR conductivity in the normal and superconducting states. This quantity is obtained by subtracting the calculated free-carrier contribution (shown in Fig. 8 as solid lines) from the total conductivity. Some features that are common at all temperatures include an onset near 80 cm^{-1}, a maximum around 250 cm^{-1}, a notchlike structure at 400 cm^{-1}, and a broad peak around 800 cm^{-1}. As we can see, the MIR conductivity $\sigma_{1MIR}(\omega,T)$ has a relatively weak temperature dependence. There do appear to be three distinct temperature regimes: >250 K, T_c-200 K, and below T_c. In each, there is a noticeable conductivity increase in the region of 150–1500 cm^{-1} compared to the higher-temperature regime. The enhancement is more obvious for $T<T_c$ and will be discussed below.

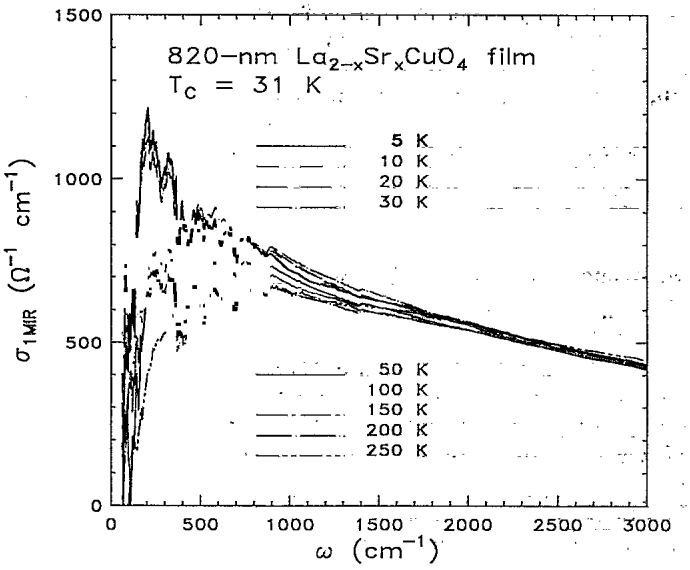

FIG. 10. σ_{1MIR}, the frequency-dependent conductivity with Drude contribution subtracted. The data fall into three groups, 5–T_c, T_c–200, and ≥ 250 K.

According to the data in Fig. 10, the "two-feature" structure of an onset near 80 cm^{-1} ($3.7k_BT_c$) and a notch around 400 cm^{-1} ($18k_BT_c$) is present both below and above T_c. This structure is shown more clearly in Fig. 11, where we plot the average of the curves above and below T_c. Thus, we cannot associate either feature with the superconducting gap, since that presumably would not appear above T_c. Furthermore, there is no shift in any feature in the superconducting state as would be expected for a Holstein sideband associated with the condensate. Such features have also been observed[32,57,62] in $YBa_2Cu_3O_{7-\delta}$ and $Bi_2Sr_2CaCu_2O_8$ films. The structure at 400 cm^{-1} (50 meV), which appears common to the cuprate superconductors, has been explained as due to strong bound-carrier–phonon coupling.[63] It cannot be accepted as a superconducting gap for $La_{2-x}Sr_xCuO_4$ simply because its magnitude is too large. The value of the lower-energy onset usually varies for different samples. The presence of this structure above T_c and the lack of evidence of an energy shift with varying temperature below T_c make it difficult to associate it with the BCS gap.

3. *Holstein effect*

Lee, Rainer, and Zimmermann[64] have calculated the dynamic conductivity in the framework of strong-coupling theory, including the Holstein mechanism.[65,66] They obtain a two-gap structure in the superconducting state. The first onset is presumed to be the superconducting gap, while the "second gap" is interpreted as the consequence of inelastic scattering with phonons due to the Holstein effect.

To estimate this effect, we have calculated the conductivity according to the Holstein theory for our film and

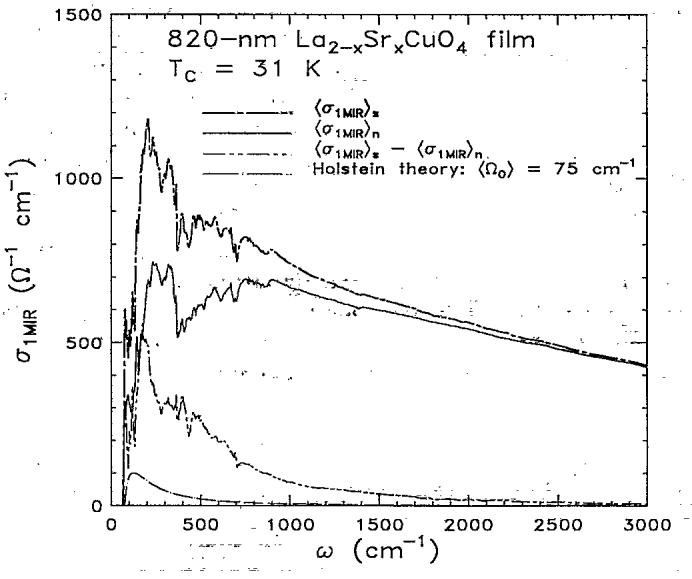

FIG. 11. Averaged midinfrared conductivity in the normal and superconducting states. Also shown is the difference between them. The dash-dotted curve is a calculation within the framework of Holstein theory.

find that the enhancement of the MIR strength below T_c may not be accounted for by the inelastic-scattering contribution. In the Holstein model, the scattering rate at low temperature can be obtained by[66]

$$1/\tau(\omega)=\frac{2\pi}{\omega}\int_0^{\omega}\alpha^2F(\Omega)(\omega-\Omega)d\Omega\ , \tag{7}$$

where $\alpha^2F(\Omega)$ is the Eliashberg function or electron-phonon spectral density. The parameters used in our calculation were $\omega_p=6300\ \mathrm{cm}^{-1}$ (from the two-component model fit outlined above), $\lambda(\omega=0)=0.25$, and the average boson frequency $\Omega_0=75\ \mathrm{cm}^{-1}$. In general, the coupling parameter is given by[66]

$$\lambda(\omega)=-\frac{2}{\omega}\int_0^{\infty}\alpha^2F(\Omega)\left[\ln\left|\frac{\omega-\Omega}{\omega+\Omega}\right|-\frac{\Omega}{\omega}\ln\left|\frac{\omega^2-\Omega^2}{\Omega^2}\right|\right]d\Omega \tag{8}$$

with a zero-frequency limiting value

$$\lambda(\omega\rightarrow 0)=2\int_0^{\infty}\frac{\alpha^2F(\Omega)}{\Omega}d\Omega\ . \tag{9}$$

For simplicity, we have assumed the Eliashberg function has the form (in an Einstein model) $\alpha^2F(\Omega)=A\delta(\Omega-\Omega_0)$, where $A=\frac{1}{2}\lambda\Omega_0$ according to Eq. (9). The calculated result is illustrated as the dash-dotted curve in Fig. 11. The size of the Holstein sideband could be enlarged to match the measured MIR spectral weight by increasing λ and ω_p, but this would be in disagreement with the values determined experimentally.

4. *Superconducting-to-normal ratios*

Another unconventional behavior is seen in the superconducting to normal-state conductivity ratio shown in Fig. 12. Ratios of conductivity have been used frequently in the past to suggest superconducting gap structure.[49,52] In Fig. 12, we compare σ_{1s} and "σ_{1n}" at the *same* temperature (we note that if σ_{1s} and σ_{1n} are compared at *different* temperatures, the result is totally different as shown in the inset, resembling the BCS-like behavior). To estimate $\sigma_{1n}(\omega,T)$ below T_c, we presume that the "normal state" ω_{pD} and $1/\tau$ below T_c follow the "normal" behavior, i.e., ω_{pD} remains a constant (6300 cm^{-1}) and $1/\tau$ follows the linear extrapolation of the relaxation rate above T_c. Then σ_{1n} below T_c can be calculated as the sum of the calculated Drude component and the averaged MIR conductivity $\langle\sigma_{1\mathrm{MIR}}\rangle_n$, namely,

$$\sigma_{1n}=\begin{cases}\text{measured } \sigma_1, & T>T_c\ ,\\ \dfrac{1}{4\pi}\dfrac{\omega_{pD}^2\tau}{1+\omega^2\tau^2}+\langle\sigma_{1\mathrm{MIR}}\rangle_n, & T<T_c\ .\end{cases} \tag{10}$$

As we can see in Fig. 12, the ratio σ_{1s}/σ_{1n} exhibits a sharp edge near 100 cm^{-1} and has a peak around 180 cm^{-1}. The peak is suppressed but does not shift as T approaches T_c from below. σ_{1s} "overshoots" σ_{1n} up to 1000 cm^{-1} and then gradually joins the normal-state conductivity at higher frequencies. This surprising result can be attributed first to the observed enhancement of the midinfrared conductivity in the superconducting state, and second to the observed faster-than-linear decrease in the quasiparticle scattering rate as demonstrated in Fig. 9.

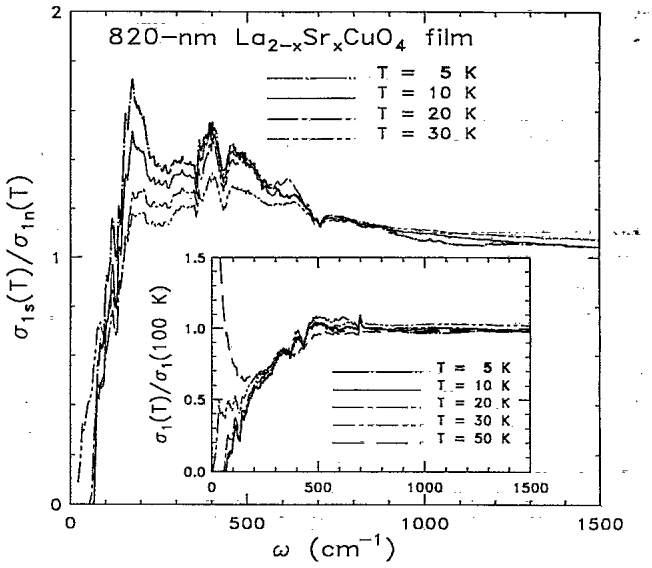

FIG. 12. The ratio of the real part of the conductivity in the superconducting state to an estimated normal-state conductivity at the *same* temperature. For comparison, the inset demonstrates the ratio of the conductivity at a temperature T to that at a *fixed* temperature of 100 K.

5. *Extra spectral weight below T_c*

We turn to the differences between the MIR conductivity above and below T_c. An enhancement is evident in the raw data of Fig. 5, in which we can see the conductivity at 5 K is higher than that at 50 K, above T_c, for $\omega\gtrsim 360\ \mathrm{cm}^{-1}$. By calculating the difference between the averaged midinfrared conductivity in the superconducting state, $\langle\sigma_{1\mathrm{MIR}}\rangle_s$, and the one in the normal state, $\langle\sigma_{1\mathrm{MIR}}\rangle_n$, we find an extra spectral weight below T_c in the MIR region which accounts for roughly 15% of the Drude oscillator strength. This difference is shown in Fig. 11. (Note that the actual fraction may be smaller for the reason of large error bars in σ_1 at low ω below T_c, as will be discussed below; thus the difference, $\langle\sigma_{1\mathrm{MIR}}\rangle^{bs}-\langle\sigma_{1\mathrm{MIR}}\rangle_n$, may be exaggerated at low frequencies.) This anomalous behavior suggests the existence of another type of excitation visible in the superconducting state, with the normal Drude carriers not completely condensing into the superfluid below T_c. However, this argument cannot be taken as rigorous, since our approach of extracting the Drude component has neglected the ω dependence of the electronic scattering rate, though it may be weak as suggested by the small value of coupling constant $\lambda\sim 0.25$.

To confirm our observation of the extra spectral weight below T_c in the MIR conductivity obtained by the two-component analysis, we use two other independent

methods to estimate the oscillator strength of the superconductor condensate: the dielectric function and the f-sum rule. According to the clean-limit picture, when $2\Delta \gg 1/\tau$ the Drude oscillator strength will condense into a $\omega=0$ δ function for $T \ll T_c$. Thus, the real part of the dielectric function at low frequencies is

$$\epsilon_1(\omega)=\epsilon_{1b}-\frac{\omega_{ps}^2}{\omega^2}\ , \qquad (11)$$

where ω_{ps} is the superconducting plasma frequency defined as $\omega_{ps}=4\pi n_s e^2/m_b$ with n_s being the density of superfluid carriers of mass m_b; and ϵ_{1b} is the bound-carrier contribution to $\epsilon_1(\omega)$, i.e., the low-frequency sum of all finite frequency absorption. In principle, ϵ_{1b} is ω dependent. It is constant only at frequencies well below the lowest bound-carrier resonant frequency.

Figure 13 shows the plot of $\epsilon_1(\omega)$ [obtained from KK transform of $\mathcal{R}(\omega)$] against ω^{-2}. The data fall on a straight line, as predicted by Eq. (11), in the low-frequency range. The slope obtained from a linear regression fit at $T=5$ K gives $\omega_{ps} \approx 5800 \pm 100$ cm^{-1}, from which the London penetration depth can be estimated to be $\lambda_L = 1/2\pi\omega_{ps} = 275 \pm 5$ nm. This value, which is much less than the film thickness (820 nm), is comparable to the 250 nm in-plane λ_L found by muon-spin-relaxation (μSR) measurements[67] for $La_{1.85}Sr_{0.15}CuO_4$ at $T=6$ K. We note that only a fraction $f_s=\omega_{ps}^2/\omega_{pD}^2 \approx 85\%$ of the free carriers condense into the superfluid, in agreement with the observation that $\sim 15\%$ of the Drude spectral weight has shifted to the MIR region below T_c as outlined above. Further evidence that supports this argument is obtained from the f-sum rule that will be discussed next.

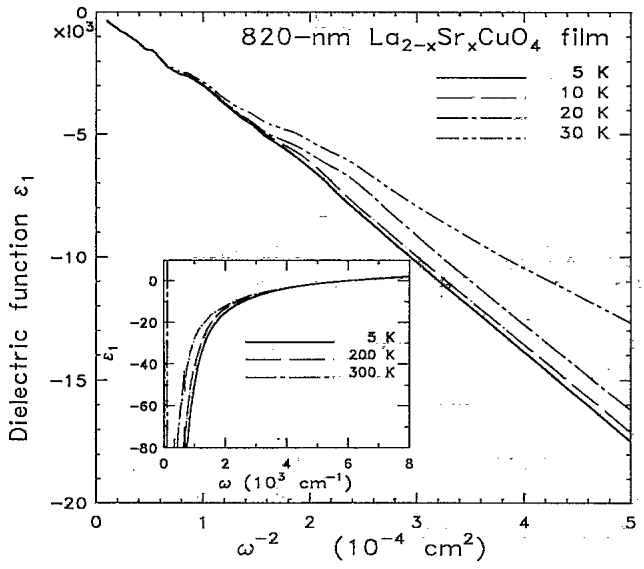

FIG. 13. Real part of the dielectric function ϵ_1 against ω^{-2} below T_c. The frequency range shown is 45–300 cm^{-1}. Inset: ϵ_1 vs ω at 5, 200, and 300 K, illustrating the ω-dependent metallic response and the zero-crossing near the plasma edge (~ 6000 cm^{-1}).

C. Sum rule: Superconducting condensate

Figure 14 illustrates the spectral weight, $N_{\rm eff}(\omega)m/m_b$, as defined according to

$$N_{\rm eff}(\omega)\frac{m}{m_b}=\frac{2mV_{\rm cell}}{\pi e^2}\int_0^{\omega}\sigma(\omega')d\omega'\ , \qquad (12)$$

where e and m are the free-electron charge and mass, respectively. m_b is the averaged high-frequency optical or band mass, and $V_{\rm cell}$ is the volume (95 Å^3) of one formula unit. In this expression, $N_{\rm eff}(\omega)$ equals to the effective number of carriers per formula unit participating in optical transition at frequencies below ω.[37] The normal-state $N_{\rm eff}(\omega)$ curves at 10000 cm^{-1} give, if $m_b=m$, roughly 0.18 hole per CuO_2 layer, which is a value close to the dopant concentration of our film ($x \sim 0.17$) assuming each Sr atom donates one hole to the CuO_2 layer.

In the normal state, the curves exhibit a sharp rise in the far infrared followed by a broad plateau before another rise beginning near 10000 cm^{-1} due to the charge-transfer transition. As the temperature is lowered, spectral weight transfers to lower frequency in response to a decreasing relaxation rate. Below T_c, the spectral weight is reduced as expected due to superconducting condensation. From the difference between $N_{\rm eff}(\omega)m/m_b$ for the normal and the superconducting states, the plasma frequency of the superfluid charge carriers [or the missing area in the curve of $\sigma_1(\omega)$] can be estimated. This difference gives $\Delta(N_{\rm eff}m/m_b)=\omega_{ps}^2 mV_{\rm cell}/4\pi e^2$, from

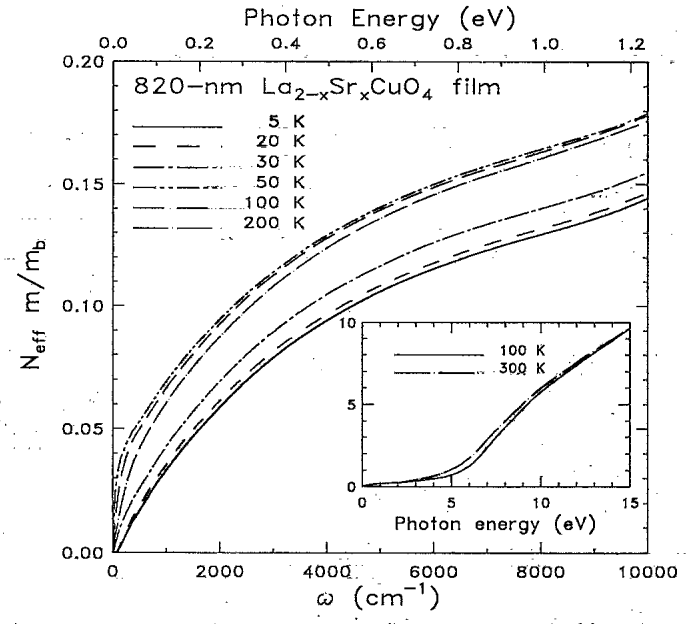

FIG. 14. Effective carrier density per Cu atom, $N_{\rm eff}m/m_b$, as a function of frequency for various temperatures. The data are obtained from the area under the curves of $\sigma_1(\omega)$. The spectral weight of the superfluid condensate can be estimated from the difference of $N_{\rm eff}m/m_b$ in the normal and superconducting states. The inset illustrates the behavior at higher energy for $T=100$ and 300 K where the high-frequency reflectivity data of Tajima *et al.* (Ref. 19) have been utilized.

which we find $\omega_{ps}=5800$ cm^{-1} at 5 K, in excellent agreement with the value determined from the real dielectric function as discussed earlier.

One surprising result of our measurements is that the $N_{\rm eff}(\omega)m/m_b$ in the charge-transfer region is larger at $T\geq 300$ K than at other temperatures below 250 K, as shown in the inset of Fig. 14. The mechanism that causes this difference is not clear at this moment. One speculation is that the structural transition at around 250 K may change the band structure due to the doubling of the unit cell. The transformation introduces new Brillouin zone planes at which the semiconductorlike gaps are opened, transferring oscillator strength to higher-frequency regions. The band mass may also charge accordingly. Our choice of extrapolation makes this difference disappear above 15 eV, where the $N_{\rm eff}(\omega)m/m_b$ curves come together. 15 eV is the end point of the interband excitations from the O $2p$ valence bands to the La $5d/4f$ conduction bands above the Fermi level and the starting point of excitations from the Cu $3d$ bands to the La $5d/4f$ bands.

Figure 15 shows the temperature dependence of the Drude (ω_{pD}) and superconducting (ω_{ps}) plasma frequencies. Here ω_{pD} is determined from the fit to $\sigma_1(\omega)$ as described earlier and is consistent with a picture of constant carrier concentration in the normal state. This magnitude of ω_{pD} ($\sim$0.8 eV) is smaller in comparison with the values ($\sim$1.2 eV) obtained in YBCO or BiSrCaCuO crystals, presumably indicating lower carrier concentration on the CuO_2 planes. Below T_c, ω_{ps} is estimated from the sum rule, the linear fit to $\epsilon_1(\omega)$ vs ω^{-2}, and the least-squares fit to the reflectance data using a two-fluid model. These three approaches give very close results in ω_{ps} and we take the average value. Shown in the inset is the superfluid electronic density fraction $f_s(T)$. This superconducting condensate is calculated according to

$$f_s(T)=n_s(T)/n=\omega_{ps}^2(T)/\omega_{pD}^2$$

with $\omega_{pD}=6300$ cm^{-1}, the normal-state value. This quantity $f_s(T)$ is essentially a measure of the strength of the δ function in $\sigma_1(\omega,T)$, and is related to the T dependence of the penetration depth $\lambda_L(T)$. The solid curves in Fig. 15 and its inset show the phenomenological behavior predicted by BCS theory according to

$$\frac{f_s(T)}{f_s(0)}=\left[\frac{\Delta(T)}{\Delta(0)}\right]^2, \tag{13}$$

where $\Delta(T)$ is the T-dependent BCS order parameter. It gives a nearly constant $\Delta(T)$ at $T\ll T_c$. Near T_c, $\Delta(T)$ drops to zero with a $(1-T/T_c)^{1/2}$ dependence. The behavior of $f_s(T)$ in our data agrees with this expression and it demonstrates that the normal carriers condense rapidly into the superfluid below T_c, as expected.

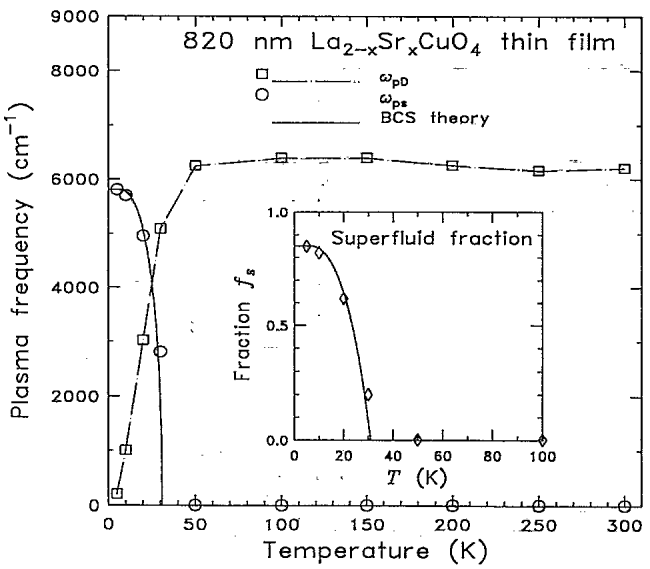

FIG. 15. Temperature dependence of the Drude plasma frequency $\omega_{pD}(T)$, the superconducting plasma frequency $\omega_{ps}(T)$, and the superfluid density $f_s(T)=n_s(T)/n$. The solid lines are calculated in the framework of BCS theory, taking $f_s(0)=0.85$ and $T_c=31$ K.

D. One-component approach

An alternative approach to analysis of the optical conductivity is the one-component model with a frequency-dependent mass and scattering rate.[53,68–70] In this approach, the infrared absorption is entirely due to free carriers, in which are divided into "coherent" and "incoherent" parts caused by the interaction of the free carriers with some sort of optically inactive excitations (charge or spin fluctuations).[62] This approach has been proposed by Anderson[71] and applied to heavy-fermion superconductors.[72] The normal Drude component is regarded as the coherent part centered at $\omega=0$. The incoherent part occurs at frequencies characteristic of the excitations and shifts away from $\omega=0$ due to interactions with the excitations. In this model, the complex dielectric function is described by a generalized Drude formula:

$$\epsilon(\omega)=\epsilon_h-\frac{\omega_p^2}{\omega[\omega-\Sigma(\omega)]}, \tag{14}$$

where ϵ_h is the "background" dielectric associated with the high-frequency contributions, ω_p—defined by $4\pi Ne^2/m_b$—is the bare plasma frequency of the free carriers, and $\Sigma(\omega)=\Sigma_1(\omega)+i\Sigma_2(\omega)$ is the self-energy of the carriers.

Because $\epsilon(\omega)$ is causal, $\Sigma_1(\omega)$ and $\Sigma_2(\omega)$ are related by the Kramers-Kronig equations. It is important to stress that the interband contributions, which can be lumped into ϵ_h, are excluded from ω_p and $\Sigma(\omega)$. To find $\Sigma(\omega)$, knowledge of ω_p and ϵ_h is required. In order to identify the interband components, we fit the experimental $\sigma_1(\omega)$ at frequencies higher than 800 cm^{-1} with Lorentz oscillators to parametrize the interband absorption. By subtracting the contribution due to these interband oscillators from the total conductivity and calculating the area under $\sigma_1(\omega)$, we obtain $\omega_p=13\,000$ cm^{-1}, corresponding to a carrier density of $n=1.8\times10^{21}$ cm$^{-3}(m_b/m)$ or 0.17 holes per CuO_2 unit if $m_b=m$. As we have found $\omega_{pD}=6300\pm100$ cm^{-1} in the two-component analysis, we

can also estimate the strength of MIR absorption or the "incoherent" component as

$$\omega_{pm}=(\omega_p^2-\omega_{pD}^2)^{1/2}\approx 11\,370\ \mathrm{cm}^{-1}\ .$$

ϵ_h can be estimated from the interband oscillators. This gives $\epsilon_h\sim 4$ in the far-infrared region; at higher frequencies ϵ_h becomes complex and ω dependent.

1. *Mass enhancement m^*/m_b and self-energy $\Sigma(\omega)$*

Once ω_p and ϵ_h are determined, the self-energy $\Sigma(\omega)$ can be calculated at each frequency from the experimental $\epsilon(\omega)$ according to Eq. (14). If we rewrite Eq. (14) as

$$\epsilon(\omega)=\epsilon_h-\frac{\omega_p^{*2}}{\omega[\omega+i/\tau^*(\omega)]} \qquad (15)$$

and compare Eq. (15) with Eq. (14), we can extract the renormalized scattering rate $1/\tau^*(\omega)=-\Sigma_2(\omega)m_b/m^*$, and the effective plasma frequency $\omega_p^*=\omega_p(m_b/m^*)^{1/2}$, where the effective mass enhancement is given by

$$m^*/m_b=1-\Sigma_1/\omega\ . \qquad (16)$$

Note both the real and imaginary parts of $\Sigma(\omega)$ are negative definite. The resulting curves of $m^*(\omega)/m_b$ and $\Sigma_2(\omega)$ are shown in Fig. 16. The effective mass m^* is greatly enhanced at low ω and $m^*\approx m_b$ at high ω, as expected for the MFL and NFL theories.[34,35]

The behavior of $m^*(\omega)/m_b$ and $\Sigma_2(\omega)$ as shown can be viewed as arising from a local Coulomb interaction of carriers with a broad spectrum of other excitations. At low frequencies, the carriers drag a low-energy excitation cloud along with them, causing a mass enhancement. As frequency increases, the scattering rate $1/\tau^*$ increases when the low-lying states are excited; hence, a new *inelastic* scattering occurs. The carrier mass decreases to approach the band mass as ω increases, for the low-lying excitations cannot follow the rapid carrier motion. We can estimate the characteristic energy range of the low-lying excitations from the frequencies at which $m^*(\omega)$ and $\Sigma_2(\omega)$ change from their low- to high-frequency behaviors. This range appears to be between 300 and 1000 cm^{-1} (0.04–1.2 eV). We note that a pronounced peak near 0.1 eV reported by Uchida *et al.*[21] is not observed in our spectra of m^*/m_b and Σ_2. The present values of Σ_2 are comparable with their result for the unnormalized scattering rate. The mass enhancement here is, however, a factor of 0.15 smaller than their result. The high value of m^* in their data would imply an even stronger coupling between the free carriers and the low-lying excitations, which is difficult to understand. Note that the value of m^*/m_b at low ω and low T can also be predicted from the conductivity sum rule from Fig. 14 or simply from $\omega_p^2/\omega_{pD}^2\sim 4.2$, which agrees well with the result in Fig. 16. Writing $m^*/m_b=1+\lambda$, we find the low-frequency limit value of coupling constant $\lambda\approx 3$ at low temperatures, suggesting strong interaction of carriers with a spectrum of other excitations. One major difficulty with this model is that this large λ would give a high T_c, inconsistent with the actually measured T_c value.

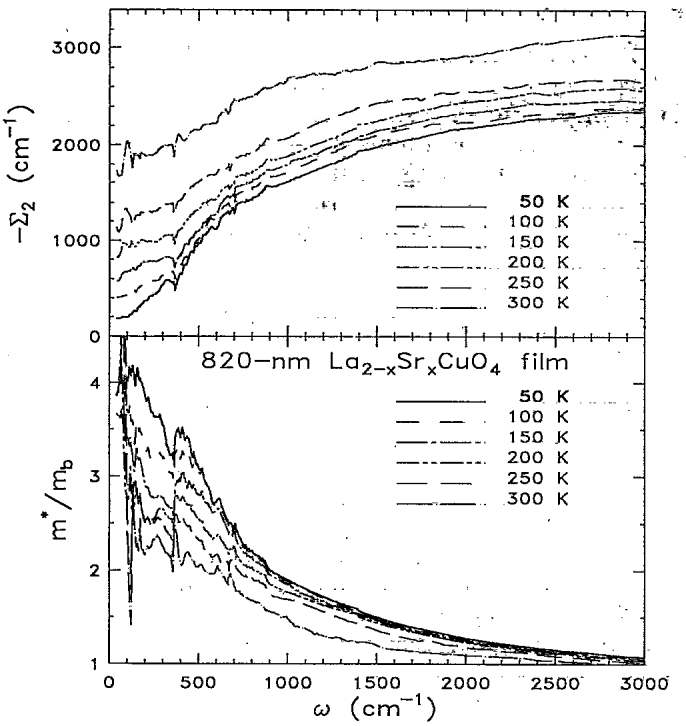

FIG. 16. Frequency-dependent mass enhancement (lower panel) and imaginary part of the self-energy (upper panel) derived from the experimental complex dielectric function with interband contributions subtracted.

2. *Effective scattering rate $1/\tau^*(\omega)$*

A linear T-dependent scattering rate at $\omega\sim 0$ implies it is also linear in ω at higher frequencies. The effective renormalized scattering rate can be obtained by $1/\tau^*=-(m_b/m^*)\Sigma_2$. This quantity is shown in Fig. 17. The extrapolated $\omega=0$ values of $1/\tau^*$ are compatible to those obtained above in the two-component fit by assuming a constant scattering rate. This is not surprising since both the one- and two-component approaches have described the dc transport behavior well. At higher frequencies, we observe $1/\tau^*$ is of order $\max(T,\omega)$ before it saturates. According to the MFL theory, however, it is not $1/\tau^*$ but the imaginary part of the quasiparticle self-energy Σ_2 that has the form $-\Sigma_2=\lambda\max(\pi T,\omega)$, as long as $\omega<\omega_c\simeq 1000\ \mathrm{cm}^{-1}$. Thus, Σ_2 would change from constant to linear in ω at $\omega>\pi T$. At low ω, our results agree with this prediction, and Σ_2 tends to saturate at frequencies above ω_c. Since λ is, in principle, T independent, one expects the slope of $\Sigma_2(\omega)$ to be constant at all temperatures in MFL theory. However, our data indicate a gradual decrease of slope with increasing temperature.

It is difficult to interpret the frequency-dependent scattering rate as a consequence of inelastic scattering due to the Holstein effect,[65,66] in which a carrier can absorb a photon of energy $\hbar\omega$, emit an excitation (or a phonon) of energy ε ($\varepsilon\sim 300\ \mathrm{cm}^{-1}$ in this case), and scatter. First, the large value of λ (~ 3) implied by the analysis of

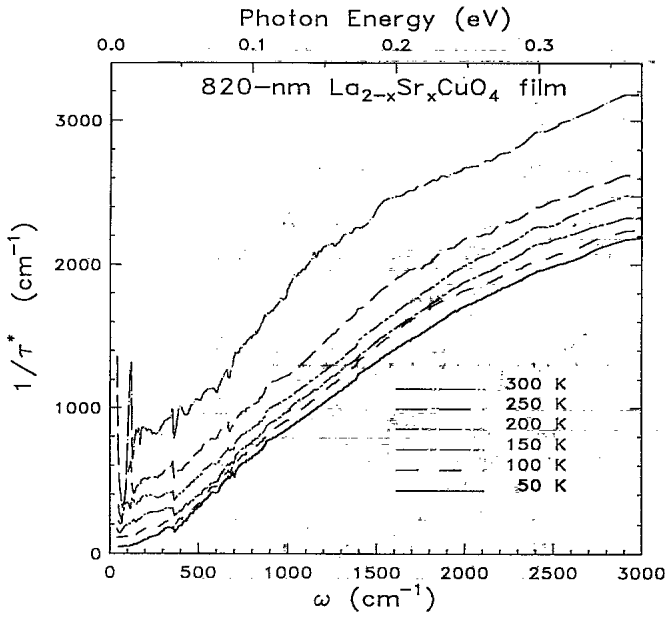

FIG. 17. Renormalized scattering rate given by $1/\tau^* = -(m_b/m^*)\Sigma_2$.

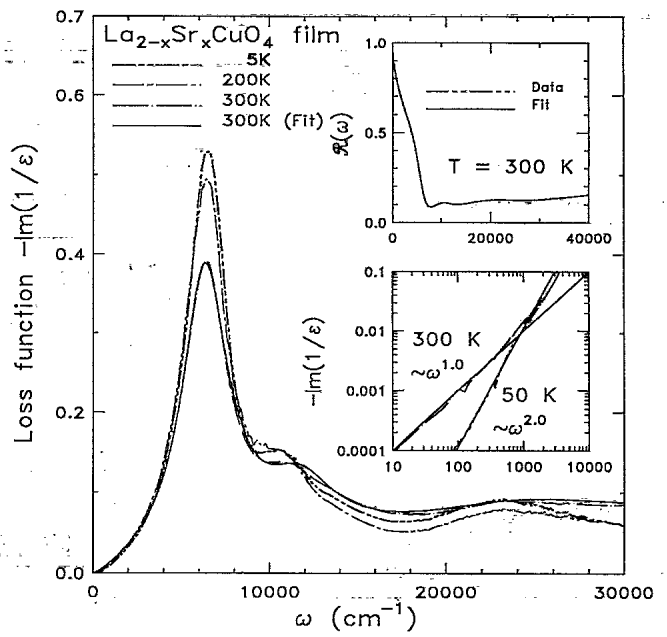

FIG. 18. Energy-loss function calculated from the Kramers-Kronig analysis of $\mathcal{R}(\omega)$ at selected temperatures. The solid line is a calculation using the oscillator parameters obtained from a two-component model fit to $\mathcal{R}(\omega)$ as shown in the upper inset. The lower inset illustrates the different low ω-dependent behavior of the loss function at 50 and 300 K.

Fig. 16 suggests a strong coupling between the conduction carriers and the excitation. Therefore, at $T > \varepsilon \sim 400$ K, the dc resistivity should significantly deviate from its linear T-dependent behavior. Such a large λ would also imply that the mean free path is of the same order of the lattice constant at room temperature, thus the dc resistivity would be expected to saturate, inconsistent with the observed linear behavior which persists up to 1100 K for LSCO materials.[24] Second, the Holstein sideband would shift upwards by 2Δ, the threshold energy for exciting two quasiparticles, in the superconducting state. On the contrary, our spectra in Fig. 5 do not show such shift. However, this structure could have been smeared out as the size of the Holstein effect depends sensitively on the shape of the Eliashberg function $\alpha^2F(\Omega)$ and on impurity scattering.[64] The possibility of a Holstein effect therefore may not be completely ruled out.

E. Loss function

In the temperature-dependent reflectance spectra of Figs. 3 and 4, we have observed that the reflectivity edge sharpens and slightly moves to higher frequency with decreasing temperature. This may be attributed mainly to the effect of volume contraction. The behavior can also be seen in the electronic loss function $-\mathrm{Im}(1/\epsilon)$ as demonstrated in Fig. 18. Upon cooling, the peak position at the screened plasma frequency $\tilde{\omega}_p \approx 6400$ cm^{-1} (~ 0.8 eV) shifts to slightly higher energies along with a slight narrowing of the broad peak. This can be understood in terms of the generalized Drude model, in which the maximum value in $-\mathrm{Im}(1/\epsilon)$ is given approximately by $\tilde{\omega}_p\tau^*/\epsilon_h$ at $\omega = \tilde{\omega}_p \approx \omega_p/\sqrt{\epsilon_h}$ with a width of $1/\tau^*(\tilde{\omega}_p)$. This broad width (0.4 eV) is caused by the anomalous midinfrared background absorption.

Bozovic[73] found that $-\mathrm{Im}(1/\epsilon) = \beta\omega^2$ for small ω in both Y-Ba-Cu-O and Bi-Sr-Ca-Cu-O, and conjectured that the quadratic law was universal for all layered cuprate superconductors. In addition, it has been suggested that the two-component oscillator model fails to reproduce accurately the experimental loss function.[73] After making careful analysis on our $La_{2-x}Sr_xCuO_4$ film, however, we find our results are in sharp contrast to these conclusions. By using the dielectric function with a two-component model in the form of Eq. (1) to fit the room-temperature reflectance, we obtain a set of oscillator parameters which can almost exactly reproduce the measured $\mathcal{R}(\omega)$ as shown in the upper inset to Fig. 18. The oscillator parameters are listed in Table II. When the same set of parameters is used to calculate the loss function, we can see an excellent agreement with the experimental $-\mathrm{Im}(1/\epsilon)$ curve throughout the entire measured range as illustrated in the main part of Fig. 18. We want to stress here that the peak in $-\mathrm{Im}(1/\epsilon)$ is determined not only by the free carriers, but also by the bound carriers participating the charge-transfer and interband transitions. The loss function can be well fit only after the interband oscillators are taken into account.

When looking into the small-ω behavior of the loss function, we note that for our film the low-frequency quadratic law $-\mathrm{Im}(1/\epsilon) \sim \omega^2$ suggested by Bozovic *et al.*[73,74] is valid only at low temperatures (or at higher frequencies). A linear ω dependence, instead, is more appropriate for high temperatures. The result is more evident when our data are plotted in log-log scale as shown in the lower inset of Fig. 18. This behavior can be understood quantitatively in the one-component approach.

TABLE II. Parameters of a two-component oscillator fit to the measured $\mathcal{R}(\omega)$ at room temperature. $\epsilon_\infty = 1.5$.

Oscillator no.	ω_0 (cm^{-1})	ω_p (cm^{-1})	γ (cm^{-1})
Drude	0	6240	358
Mid-IR no. 1	250	2320	210
Mid-IR no. 2	950	10640	2850
Mid-IR no. 3	3180	6580	4330
Phonon no. 1	126	750	28
Phonon no. 2	359	455	22
Phonon no. 3	681	450	25
CT band	11260	6720	4820
Interband no. 1	23650	16620	15630
Interband no. 2	59370	94290	33410

Starting with Eq. (14), one can derive the approximation for $\omega \ll \omega_p$:

$$-\mathrm{Im}(1/\epsilon) \approx -\frac{\omega\Sigma_2}{\omega_p^2} \propto -\omega\Sigma_2 , \tag{17}$$

where $\omega_p = 13000$ cm^{-1} for our film. If Σ_2 has the form of $-\Sigma_2 = \lambda \max(\pi T, \omega)$, as suggested by Fig. 16, then $-\mathrm{Im}(1/\epsilon)$ will be quadratic in ω when $T < \omega/\pi$ but linear in ω when $T > \omega/\pi$. We can see the 300-K curve in the inset changes its slope at $\omega_c \simeq 700$ $cm^{-1} \sim \pi T$, giving a $\sim\omega^2$ dependence above ω_c and an ω linear dependence below ω_c. [In fact, the 50-K curve also becomes linear in ω at frequencies below 100 $cm^{-1} \sim \pi T$ (not shown).] This behavior can also be explained qualitatively in the two-component analysis. At small ω, the dielectric function $\epsilon(\omega)$ is dominated by the Drude term, thus the loss function exhibits the ordinary ω linear dependence. At higher frequencies, the midinfrared tail becomes important, causing the loss function to deviate from this linear behavior.

F. The superconducting gap

In the conventional Bardeen-Cooper-Schreiffer superconductors,[75] it has been demonstrated successfully that the superconducting-to-normal ratio in transmission[76–78] would give a maximum very near 2Δ, the superconducting gap energy. Other experiments[79,80] showed that the gap corresponded to a threshold in surface resistance or conductivity. Many attempts have been made to identify the superconducting gap of HTSC at the peak in the reflectance ratio $\mathcal{R}_s(T)/\mathcal{R}_n$ or at the onset of the conductivity $\sigma_{1s}(\omega)$. However, it is problematic to make such assignments. First, the reflectance data (see Fig. 4, for example) do not exhibit a clear edge. Second, the phonon structure and MIR absorption tail as well as the T dependence of the scattering rate complicate this approach. Finally, the propagated errors in $\sigma_{1s}(\omega)$ at low frequencies are large due to the fact that $\mathcal{R}(\omega) \to 1$. The experimental accuracy in $\mathcal{R}(\omega)$ in the far infrared is not much better than $\pm 0.5\%$. We repeated the reflectance measurements on our sample five times, finding agreement within $\pm 0.5\%$ above 300 cm^{-1} but variations from the average up to $\pm 1\%$ at 40 cm^{-1}. This is illustrated in Fig. 19 where we plot in the upper panel the average reflectance at 5 and 200 K as solid lines. The dashed curves represent upper and lower estimates of the uncertainty in $\mathcal{R}$: $\pm 0.5\%$ at 200 K and above 300 cm^{-1} at 5 K; the highest and lowest measured reflectances below 200 cm^{-1}, with a smooth merge between 200 and 300 cm^{-1}. We can then estimate the uncertainty in $\sigma_1(\omega)$ by performing the KK transformation. The results are in the lower panel of Fig. 19. The propagated uncertainty goes roughly $\Delta\sigma_1/\sigma_1 = [1/(1-\mathcal{R})](\Delta\mathcal{R}/\mathcal{R})$, as mentioned in the end of Sec. II. As we can see, the absorption edge of $\sigma_{1s}(\omega)$, whose value ($\sim 3.7 k_B T_c$) appears to coincide with the prediction of BCS theory,[75] is largely dependent on the accuracy of $\mathcal{R}(\omega)$. This prevents any gap assignment based on the onset of σ_{1s}.

Kamarás *et al.*[32] have argued that a superconducting gap cannot be unambiguously identified in the infrared spectra if the material is in the clean limit, $1/\tau \ll 2\Delta$ or $l \gg \xi$, with l the electronic mean free path and ξ the coherence length. In our sample, the free-carrier relaxation rate is $1/\tau \sim 2.5 k_B T_c$ at 50 K ($\tau = 0.1$ ps), smaller than the expected BCS superconducting gap. One expects an even smaller value of $1/\tau$ well below T_c, thus the clean-limit condition will be met. This low free-carrier relaxation rate implies that most of the free-carrier oscillator strength would move to the zero-frequency δ function of the superconductor, leaving little strength—only a factor $1/(\pi\tau\Delta)$ of the Drude spectral weight— avail-

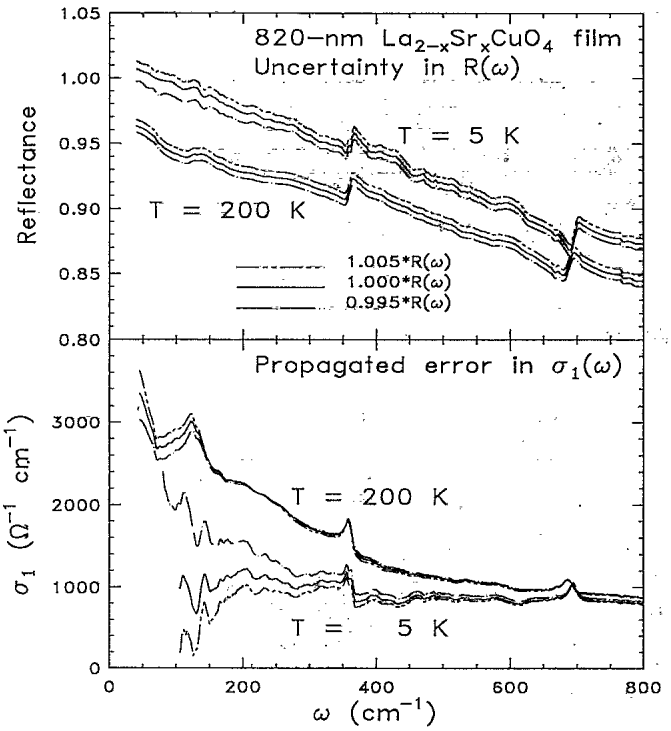

FIG. 19. The propagated uncertainty in values of the conductivity derived from the reflectance $\mathcal{R}$, in which $\mathcal{R}$ is close to unity and has the uncertainty shown.

able for the gap transition. As seen in Fig. 10, there is already considerable second-component (MIR) absorption in the low-frequency region, making it likely that any remaining gap structure is obscured by the intense midinfrared absorption.

IV. CONCLUSIONS

In this paper, we presented a set of temperature- and frequency-dependent optical spectral functions from the far-infrared through the ultraviolet region. We made a systematic analysis for an epitaxial $La_{2-x}Sr_xCuO_4$ thin film with a transition temperature $T_c=31$ K. We emphasized the two-component analysis for both the normal and superconducting states. Then we discussed the alternative of a one-component approach.

Our results show that the temperature dependence of the *ab*-plane infrared phonons is sensitive to the tetragonal-to-orthorhombic phase transition near 250 K. One anomalous behavior which appears to be associated with the structural transition is that the reflectance in the charge-transfer region is significantly depressed below 250 K, implying a shift of spectral weight to the higher-energy region. The electronic behavior is similar to that observed in other cuprate superconductors like YBCO or BiSrCaCuO crystals. On the other hand, the LSCO crystal has a lower free-carrier concentration but a higher phonon oscillator strength on the CuO_2 layers. The normal-state infrared properties of LSCO materials exhibit an extremely unusual non-Drude response over most of the infrared range. This anomalous behavior can be interpreted either by absorptions due to free and bound carriers in the two-component approach, or by a strong frequency-dependent scattering rate and a mass enhancement in a single-component approach.

The two-component picture analysis shows a narrow (of order k_BT) Drude absorption and a broad, strong midinfrared band. The Drude plasma frequency is essentially temperature independent, whereas the scattering rate is roughly linear in T in the normal state followed by a fast drop below T_c. A weak-coupling strength $\lambda\sim0.25$ is derived. The midinfrared absorption exhibits a weak temperature dependence in the normal state. In the superconducting state, the absorption is similar to the midinfrared band, but is enhanced in the 150–1500 cm^{-1} range. The superconducting condensate carries most ($\sim85\%$) of the free-carrier oscillator strength. No superconducting gap is discernible as the film is near the clean limit. The absorption edge near 80 or 400 cm^{-1} cannot be assigned as the superconducting gap and is attributed to the tail of low-energy excitations or to the strong bound-carrier–phonon coupling. The single-component picture analysis in the normal state shows a strongly frequency-dependent scattering rate of the order $k_BT+\hbar\omega$ at low frequencies and a large mass enhancement, which leads to a strong-coupling strength $\lambda\sim3$. This analysis has the features predicted by marginal Fermi liquid of nested Fermi liquid, but has a temperature dependent slope in the imaginary part of the quasiparticle self-energy.

ACKNOWLEDGMENTS

Research at the University of Florida is supported by NSF Grant No. DMR-9101676. Westinghouse was supported in part by AFOSR through Contract No. F49620-91-C-0034.

*Present address: Department of Physics, Virginia Tech, Blacksburg, VA 24061.

[1]J. G. Bednorz and K. A. Müller, Z. Phys. B **64**, 189 (1986).

[2]M. K. Wu, J. R. Ashburn, C. J. Tong, P. H. Hor, R. L. Meng, L. Gao, Z. J. Huang, Y. Q. Wang, and C. W. Chu, Phys. Rev. Lett. **58**, 908 (1987).

[3]T. Timusk and D. B. Tanner, in *Physical Properties of High Temperature Superconductors I,* edited by D. M. Ginsberg (World Scientific, Singapore, 1989), p. 339.

[4]G. A. Thomas, in *Proceedings of the Thirty-Ninth Scottish Universities Summer School in Physics of High-Temperature Superconductivity,* edited by D. P. Tunstall and W. Barford (Hilger, Bristol, 1991), p. 169.

[5]D. B. Tanner and T. Timusk, in *Physical Properties of High Temperature Superconductors III,* edited by D. M. Ginsberg, (World Scientific, Singapore, 1992), p. 363.

[6]K. F. Renk, in *Studies of High Temperature Superconductors,* edited by A. V. Narlikar (Nova Science, New York, 1991), Vol. 10.

[7]B. Koch, H. P. Geserich, and T. Wolf, Solid State Commun. **71**, 495 (1989).

[8]Z. Schlesinger, R. T. Collins, F. Holtzberg, C. Feild, S. H. Blanton, U. Welp, G. W. Crabtree, Y. Fang, and J. Z. Liu, Phys. Rev. Lett. **65**, 801 (1990).

[9]D. A. Bonn, J. E. Greedan, C. V. Stager, T. Timusk, M. G. Doss, S. L. Herr, K. Kamarás, C. D. Porter, D. B. Tanner, J. M. Tarascon, W. R. McKinnon, and L. H. Greene, Phys. Rev. B **35**, 8843 (1987); S. L. Herr, K. Kamarás, C. D. Porter, M. G. Doss, D. B. Tanner, D. A. Bonn, J. E. Greedan, C. V. Stager, and T. Timusk, *ibid.* **36**, 733 (1987).

[10]J. Orenstein, G. A. Thomas, D. H. Rapkine, C. G. Bethea, B. F. Levine, R. J. Cava, E. A. Reitman, and D. W. Johnson, Jr., Phys. Rev. B **36**, 729 (1987); J. Orenstein, G. A. Thomas, D. H. Rapkine, C. G. Bethea, B. F. Levine, B. Batlogg, R. J. Cava, D. W. Johnson, Jr., and E. A. Reitman, *ibid.* **36**, 8892 (1987).

[11]Z. Schlesinger, R. T. Collins, M. W. Shafer, and E. M. Engler, Phys. Rev. B **36**, 5275 (1987); Z. Schlesinger, R. L. Greene, J. G. Bednorz, and K. A. Müller, *ibid.* **35**, 5334 (1987).

[12]G. A. Thomas, A. J. Millis, R. N. Bhatt, R. J. Cava, and E. A. Rietman, Phys. Rev. B **36**, 736 (1987).

[13]U. Walter, M. S. Sherwin, A. Stacy, P. L. Richards, and A. Zettl, Phys. Rev. B **35**, 5327 (1987).

[14]G. L. Doll, J. T. Nicholls, M. S. Dresselhaus, A. M. Rao, J. M. Zhang, G. W. Lehman, P. C. Eklund, G. Dresselhaus, and A. J. Strauss, Phys. Rev. B **38**, 8850 (1988).

[15]S. Etemad, D. E. Aspnes, M. K. Kelly, R. Thompson, J. M. Tarascon, and G. W. Hull, Phys. Rev. B **37**, 3396 (1988).

[16]J. Tanaka, M. Shimada, U. Mizutani, and M. Hasegawa, Physica C **153-155**, 651 (1988).

[17]S. Tajima, S. Uchida, H. Ishii, H. Takagi, S. Tanaka, U. Kawabe, H. Hasegawa, T. Aita, and T. Ihisba, Mod. Phys. Lett. B **1**, 353 (1988).

[18]R. T. Collins, Z. Schlesinger, G. V. Chadrashekhar, and M.

W. Shafer, Phys. Rev. B **39**, 2251 (1989).
[19]S. Tajima, H. Ishii, T. Nakahashi, T. Takagi, S. Uchida, M. Seki, S. Sugai, Y. Hidaka, M. Suzuki, T. Murakami, K. Oka, and H. Unoki, J. Opt. Soc. Am. B **6**, 475 (1989).
[20]M. Suzuki, Phys. Rev. B **39**, 2312 (1989).
[21]S. Uchida, T. Ido, H. Takagi, T. Arima, Y. Tokura, and S. Tajima, Phys. Rev. B **43**, 7942 (1991).
[22]B. Batlogg, G. Kourouklis, W. Weber, R. J. Cava, A. Jayaraman, A. E. White, K. T. Short, L. W. Rupp, and E. A. Rietman, Phys. Rev. Lett. **59**, 912 (1987).
[23]T. A. Faltens, W. K. Ham, S. W. Keller, K. J. Leary, J. N. Michaels, A. M. Stacy, H.-C. zur Loye, D. E. Morris, T. W. Barbee, III, L. C. Bourne, M. L. Cohen, S. Hoen, and A. Zetle, Phys. Rev. Lett. **59**, 915 (1987).
[24]M. Gurvitch and A. T. Fiory, Phys. Rev. Lett. **59**, 1337 (1987).
[25]S. L. Cooper, G. A. Thomas, J. Orenstein, D. H. Rapkine, A. J. Millis, S.-W. Cheong, A. S. Cooper, and Z. Fisk, Phys. Rev. B **41**, 11 605 (1990).
[26]S. Tajima, S. Uchida, S. Tanaka, S. Kanabe, K. Kitazawa, and K. Fueki, Jpn. J. Appl. Phys. **26**, L432 (1987).
[27]S. L. Herr *et al.*, in *High Temperature Superconducting Materials: Preparations, Properties and Processing,* edited by William Hatfield and J. J. Miller (Marcel Dekker, New York, 1988), p. 275.
[28]D. A. Bonn, A. H. O'Reilly, J. E. Greedan, C. V. Stager, T. Timusk, K. Kamarás, and D. B. Tanner, Phys. Rev. B **37**, 1574 (1988).
[29]C. M. Foster, K. F. Voss, T. W. Hagler, D. Mihailović, A. J. Heeger, M. M. Eddy, W. L. Olsen, and E. J. Smith, Solid State Commun. **76**, 651 (1990).
[30]T. Timusk, M. Reedyk, R. Hughes, D. A. Bonn, J. D. Garrett, J. E. Greedan, C. V. Stager, D. B. Tanner, F. Gao, S. L. Herr, K. Kamarás, G. A. Thomas, S. L. Cooper, J. Orenstein, L. F. Schneemeyer, and A. J. Millis, Physica C **162-164**, 841 (1989).
[31]S. L. Cooper, G. A. Thomas, J. Orenstein, D. H. Rapkine, M. Capizzi, T. Timusk, A. J. Millis, L. F. Schneemeyer, and J. V. Waszczak, Phys. Rev. B **40**, 11 358 (1989).
[32]K. Kamarás, S. L. Herr, C. D. Porter, N. Tache, D. B. Tanner, S. Etemad, T. Venkatesan, E. Chase, A. Inam, X. D. Wu, M. S. Hedge, and B. Dutta, Phys. Rev. Lett. **64**, 84 (1990).
[33]F. Gao, G. L. Carr, C. D. Porter, D. B. Tanner, E. S. Etemad, T. Venkatesan, A. Inam, B. Dutta, X. D. Wu, G. P. Williams, and C. J. Hirschmugl, Phys. Rev. B **43**, 10 383 (1991).
[34]C. M. Varma, P. R. Littlewood, S. Schmitt-Rink, E. Abrahams, and A. Ruckenstein, Phys. Rev. Lett. **63**, 1996 (1989); **64**, 497E (1990); C. M. Varma, Int. J. Mod. Phys. B **3**, 2083 (1989); P. B. Littlewood and C. M .Varma, J. Appl. Phys. **69** 4979 (1991).
[35]A. Virosztek and J. Ruvalds, Phys. Rev. B **42**, 4064 (1990); Physica B **165&166**, 1267 (1990).
[36]J. Talvacchio, M. G. Forrester, J. R. Gavaler, and T. T. Braggins, in *Science and Technology of Thin Film Superconductors II,* edited by R. McConnel and S. A. Wolf (Plenum, New York, 1990).
[37]Frederick Wooten, *Optical Properties of Solids* (Academic, New York, 1972).
[38]S. Tajima, T. Ido, S. Ishibashi, T. Itoh, E. Eisaki, Y. Mizuo, T. Arima, H. Takagi, and S. Uchida, Phys. Rev. B **43**, 10 496 (1991).
[39]F. Gervais, P. Echegut, J. M. Bassat, and P. Odier, Phys. Rev. B **37**, 9364 (1988).
[40]R. Feile, Physica C **159**, 1 (1989).
[41]T. R. Thurson, Phys. Rev. B **39**, 4327 (1989).
[42]D. T. Keane, G. A. Held, J. L. Jordan-Sweet, M. W. Shafer, P. M. Horn, G. Guntherodt, J. Langen, M. Weit, A. Erle, S. Blumenroder, and E. Zirngiebl, Physica C **153-155**, 594 (1988).
[43]S. L. Here, K. Kamarás, D. B. Tanner, S.-W. Cheong, G. R. Stewart, and Z. Fisk, Phys. Rev. B **43**, 7847 (1991).
[44]R. P. Lowndes, Phys. Rev. B **6**, 1490 (1972).
[45]J. M. Tranquada, S. M. Heald, and A. R. Moodeneabaugh, Phys. Rev. B **36**, 8401 (1987).
[46]D. A. Bonn, J. E. Greedan, C. V. Stager, T. Timusk, M. G. Doss, S. L. Herr, K. Kamarás, and D. B. Tanner, Phys. Rev. Lett. **58**, 2249 (1987).
[47]F. Gao, D. B. Tanner, D. A. Bonn, J. E. Greedan, C. V. Stager, and T. Timusk, Bull. Am. Phys. Soc. **34**, 1036 (1989).
[48]R. Zeyher and G. Zwicknagl, Z. Phys. B **78**, 175 (1990).
[49]R. T. Collins, Z. Schlesinger, F. Holtzberg, and C. Feild, Phys. Rev. Lett. **63**, 422 (1989).
[50]B. Koch, M. Dürrler, H. P. Geserich, Th. Wolf, G. Roth, and G. Zachmann, in *Electronic Properties of High-T_c Superconductors and Related Compounds,* edited by H. Kuzmany, M. Mehrig, and J. Fink, Springer Series in Solid State Sciences, Vol. 99 (Springer-Verlag, Berlin, 1990), p. 290.
[51]K. Kamarás, C. D. Porter, M. G. Doss, S. L. Herr, D. B. Tanner, D. A. Bonn, J. E. Greedan, A. H. O'Reilly, C. V. Stager, and T. Timusk, Phys. Rev. Lett. **60**, 969 (1988).
[52]Z. Schlesinger, R. T. Collins, F. Holtzberg, C. Feild, G. Koren, and A. Gupta, Phys. Rev. B **41**, 11 237 (1990).
[53]G. A. Thomas, J. Orenstein, D. H. Rapkine, M. Capizzi, A. J. Millis, R. N. Bhatt, L. F. Schneemeyer, and J. V. Waszczak, Phys. Rev. Lett. **61**, 1313 (1988).
[54]P. B. Allen, W. E. Pickett, and H. Krakauer, Phys. Rev. B **36**, 3926 (1987).
[55]P. B. Allen, Z. Fisk, and A. Migliori, in *Physical Properties of High Temperature Superconductors I,* edited by D. M. Ginsberg (World Scientific, Singapore, 1989), p. 213.
[56]F. Gao, G. L. Carr, D. B. Tanner, S. Etemad, T. Venkatesan, B. Dutta, X. D. Wu, A. Inam, G. P. Williams, and C. J. Hirschmugl, Bull. Am. Phys. Soc. **35**, 814 (1990).
[57]D. B. Tanner, D. B. Romero, K. Kamarás, G. L. Carr, L. Forro, D. Mandrus, L. Mihály, and G. P. Williams, in *Electronic Structure and Mechanisms for High-Temperature Superconductivity,* edited by G. C. Vezolli *et al.* (Plenum, New York, 1991).
[58]D. B. Romero, C. D. Porter, D. B. Tanner, L. Forro, D. Mandrus, L. Mihaly, G. L. Carr, and G. P. Williams, Phys. Rev. Lett. **68**, 1590 (1992).
[59]J. M. Chwalek, C. Uher, J. F. Whitaker, G. A. Mourou, J. Agostinelli, and M. Lelental, Appl. Phys. Lett. **57**, 1696 (1990).
[60]E. J. Nicol and J. P. Carbotte, Phys. Rev. B **44**, 7741 (1991).
[61]M. C. Nuss, P. M. Mankiewich, M. L. O'Malley, E. H. Westerwick, and P. B. Littlewood, Phys. Rev. Lett. **66**, 3305 (1991).
[62]J. Orenstein, G. A. Thomas, A. J. Millis, S. L. Cooper, D. H. Rapkine, T. Timusk, L. F. Schneemeyer, and J. V. Waszczak, Phys. Rev. B **42**, 6342 (1990).
[63]T. Timusk and D. B. Tanner, Physica C **169**, 425 (1990).
[64]W. Lee, D. Rainer, and W. Zimmermann, Physica C **159**, 535 (1989).
[65]T. Holstein, Phys. Rev. **96**, 535 (1954); Ann. Phys. (N.Y.) **29**, 410 (1964).
[66]P. B. Allen, Phys. Rev. B **3**, 305 (1971).
[67]G. Aeppli, R. J. Cava, E. J. Ansaldo, J. H. Brewer, S. R. Kreitzman, G. M. Luke, D. R. Noakes, and R. F. Kiefl, Phys.

Rev. B **35**, 7129 (1987).
[68]R. T. Collins, Z. Schlesinger, F. Holtzberg, P. Chaudhari, and C. Feild, Phys. Rev. B **39**, 6571 (1989).
[69]L. D. Rotter, Z. Schlesinger, R. T. Collins, F. Holtzberg, C. Feild, U. Welp, G. W. Crabtree, J. Z. Liu, Y. Fang, G. Vandervoort, and S. Fleshler, Phys. Rev. Lett. **67**, 2741 (1991).
[70]S. L. Cooper, A. L. Kotz, M. A. Karlow, M. V. Klein, W. C. Lee, J. Giapintzakis, and D. M. Ginsberg, Phys. Rev. B **45**, 2549 (1992).
[71]P. W. Anderson, Mater. Res. Bull. **8**, 153 (1973); P. W. Anderson, Science **235**, 1196 (1987); P. W. Anderson, in *Frontiers and Borderlines in Many Particle Physics,* edited by J. R. Schrieffer and R. A. Broglia (North-Holland, Amsterdam, 1989); R. B. Laughlin, Science **242**, 525 (1988); P. W. Anderson, Phys. Rev. Lett. **64**, 1839 (1990).
[72]B. C. Webb, A. J. Sievers, and T. Mihalisin, Phys. Rev. Lett. **57**, 1951 (1986).
[73]Ivan Bozovic, Phys. Rev. B **42**, 1969 (1990).
[74]J. H. Kim, I. Bozovic, J. S. Harris, Jr., C. B. Eom, T. H. Geballe, W. Y. Lee, E. S. Hellman, and J. T. Cheung, Bull. Am. Phys. Soc. **37**, 283 (1992).
[75]J. Bardeen, L. N. Cooper, and J. R. Schrieffer, Phys. Rev. **108**, 1175 (1957).
[76]R. E. Glover and M. Tinkham, Phys. Rev. B **107**, 844 (1956); **108**, 243 (1957).
[77]D. M. Ginsberg and M. Tinkham, Phys. Rev. **118**, 990 (1960).
[78]P. J. M. van Bentum and P. Wyder, Physica B **138**, 23 (1986).
[79]H. D. Drew and A. J. Sievers, Phys. Rev. Lett. **19**, 697 (1967).
[80]L. H. Palmer and M. Tinkham, Phys. Rev. **165**, 588 (1968).